E3 ligase activity to the Ring1B/Mel-18 complex, and this most likely involves the recruitment of the ubiquitin-charged E2 to the complex.

Mel-18 RING Domain Is Important for Recognition of the Nucleosome

We also made mutant proteins with cysteine-to-glycine substitutions at residues 53 and 56 in the RING domain of Mel-18 (Figure 5A). These mutants also copurified normally in a complex with Ring1B (Figure 5B). However, while Ring1B/Mel-18^{C56G} ubiquitylated nucleosomes with normal efficiency (Figure 5C, lanes 2 and 4), Ring1B/Mel-18^{C53G} did not (Figure 5C, lane 3). Nevertheless, Ring1B/Mel-18^{C53G} was not completely defective, as it retained autoubiquitylation activity and the ability to ubiquitylate free histones (Figure 5C, lane 3, and Figure 5D, lanes 3–8). Therefore, in contrast to Ring1B, the RING domain of Mel-18 is not required for E3 function per se but may function specifically to mediate the interaction with its chromatin substrate.

Phosphorylation of Mel-18

Both Mel-18 purified from ES cells as well as recombinant Mel-18 migrate as several distinct bands after SDS-PAGE (Figures 6A and 6B, respectively). These are different phosophorylated forms of Mel-18, most of which disappear upon treatment with alkaline phosphatase (AP) (Figures 6A and 6B). Interestingly, in HeLa cells, the phosphorylated form of MEL-18 is associated with the chromatin fraction (Figure S5) and remains so throughout the cell cycle (Figure S6). We note that the forms of MEL-18 that are phosphorylated to a lesser extent are no longer associated with chromatin during mitosis (Figure S6B). However, it is unclear whether this represents redistribution or degradation of hypophosphorylated MEL-18.

The phosphorylated recombinant Mel-18 protein was subjected to tryptic digest and mass spectrometry. LC-MS/MS analysis led to the positive identification of two phosphopeptides where Ser132 was phosphorylated in one (minor site) and Ser254, Ser260, and Ser265 were phosphorylated in the second (Table S1). Additionally, MALDI-TOF mass spectrometry identified phosphopeptides encompassing residues 263–329 (+1–3 PO_4) and 236–329 (+2–8 PO_4) (data not shown). This was validated by inspecting the survey scans from the LTQ Orbitrap. The same peptides were observed in high charge states (5+ to 10+) at high mass accuracy (data not shown). The resultant LC-MS/MS spectra from these ions did not yield sufficiently rich fragmentation data to assign phosphorylation sites. However, after elastase digestion of a tryptic digest of Mel-18, shorter overlapping fragments of the same region of the protein were generated, and the resultant spectra permitted the assignment of phosphorylation sites at Ser110, Ser254, Ser258, Ser260, Ser265, Ser278, Thr281, Ser286, and Ser299 (Table S1). These data resolved the orbitrap survey scan result, which detected a tryptic peptide encompassing residues 236–329 with up to eight phosphorylation sites.

The location of phosphorylation sites is summarized in Figure 7A. The majority cluster in the proline/serine-rich domain at the C terminus with two sites, one of which is relatively weak, present in the central domain of the protein. Phosphorylated residues are conserved in human and mouse Mel-18 (Figure S7A), and all of the sites except Ser254 and Ser299 are also conserved in Bmi1 (Figure S7B).

Phosphorylation of Mel-18 Is Required for Ubiquitylation of Nucleosomes

We noted that both wild-type Mel-18, purified independently of Ring1B, and the Mel-18^{C53G} mutant protein exist largely in the nonphosphorylated form (Figures 2B and 5B). Since neither of these protein complexes is able to ubiquitylate nucleosomes in vitro, we reasoned that there might be a correlation between the ubiquitin ligase function of Mel-18 and its phosphorylation status.

We assayed the ubiquitin ligase activity of Ring1B/Mel-18 complex treated with AP. Whereas untreated Ring1B/Mel-18 or that treated with buffer alone ubiquitylated nucleosomes with similar high efficiency (Figure 6C, lanes 2 and 3), this was greatly diminished with the AP-treated complex (Figure 6C, lane 4). The E3 function of the MelPRC1 holocomplex purified from 293T cells showed a similar requirement for phosphorylation (Figure 6D). Importantly, the AP-treated Ring1B/Mel-18 complex retained the ability to ubiquitylate free histone proteins and also to carry out autoubiquitylation (Figure 6E, lanes 4–11 compared to lane 3), suggesting that, while E3 function is still intact, the complex was unable to recognize H2A lysine 119 in the context of the nucleosome substrate. Hence, the properties of the unphosphorylated Mel-18 directly mirror those of Mel-18^{C53G} mutant complex and suggest that, while phosphorylation does not enhance the intrinsic ubiquitin ligase function of the complex, it is required to promote recognition of the substrate.

DISCUSSION

In this study, we used affinity purification to identify human and mouse PRC1-like complexes containing MEL-18/Mel-18 (melPRC1). We show that, while melPRC1 shares common subunits with the previously described bmiPRC1, it is a functionally distinct complex. We demonstrate that melPRC1 represses *Hox* gene expression, and this correlates with its presence at the promoters of these genes. Ubiquitylation of H2A lysine 119 is associated with gene repression (Cao et al., 2005; de Napoles et al., 2004; Wang et al., 2004). In accordance, melPRC1 and a reconstituted subcomplex of melPRC1 comprising Mel-18 and Ring1B is an efficient E3 ligase in vitro and ubiquitylates H2A lysine 119 in chromatin. Mutation analysis reveals that while Ring1B plays a direct role in the ubiquitylation reaction, probably by mediating the interaction with the ubiquitin-conjugating enzyme, Mel-18 is critical for targeting the complex to lysine 119 of histone H2A in nucleosomes. Importantly, we find that, unlike bmiPRC1,

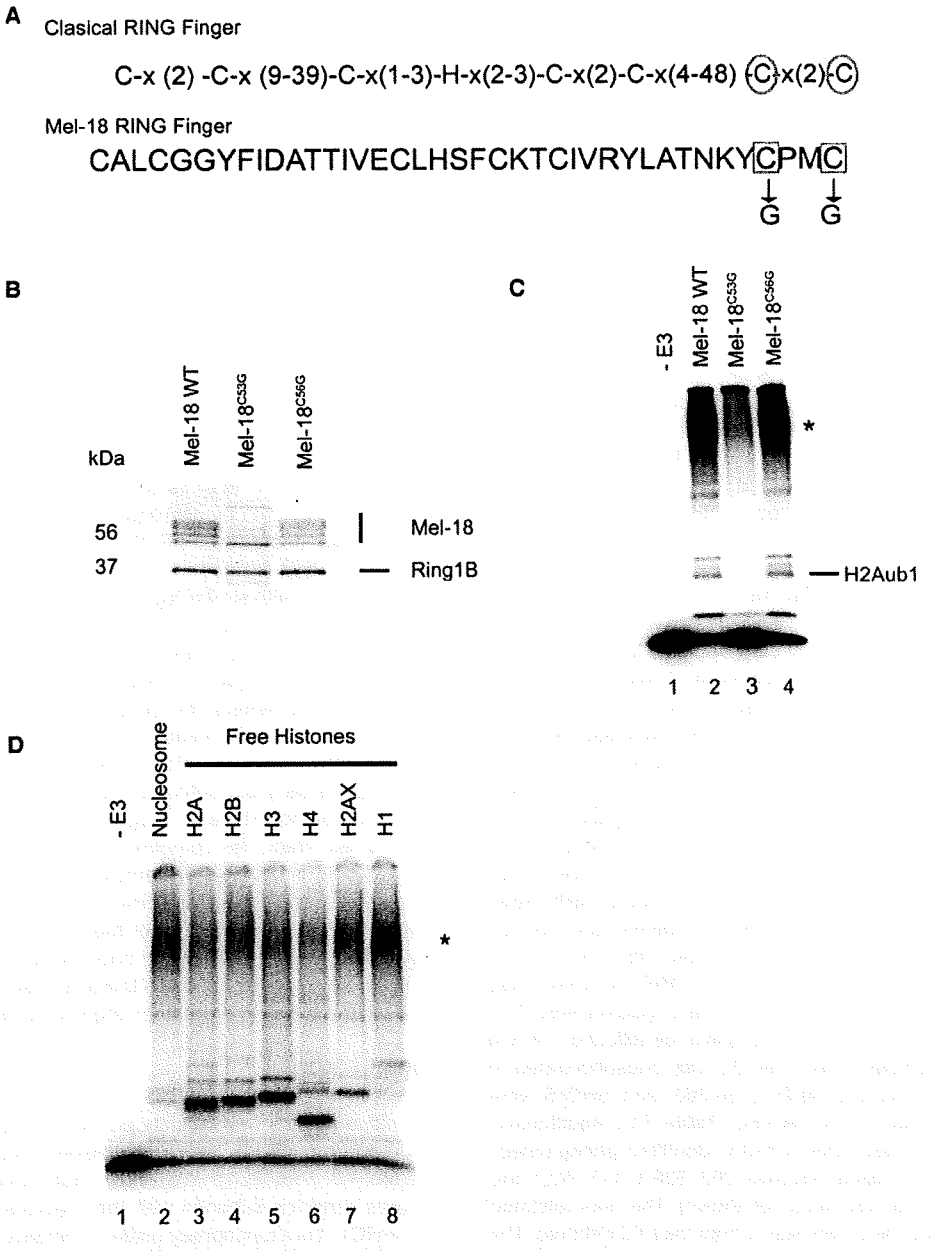

Figure 5. A Mutation in the RING Domain of Mel-18 Abolishes Ubiquitylation of Nucleosomes, but Not Free Histones

(A) Amino acid sequence of a consensus RING domain and the RING domain of Mel-18. Boxed residues represent the amino acids mutated and correspond to the circled residues of the consensus RING domain.

(B) Wild-type and mutant Ring1B/Mel-18 complexes. Molecular weight markers are indicated.

(C) Mutant Ring1B/Mel-18 complexes were examined for ubiquitylation of nucleosomes. I^{125}-ubiquitylated histone H2A (H2Aub1) and autoubiquitylated Ring1B/Mel-18 (asterix) products are indicated.

(D) Mutant Ring1B/Mel-18 complexes were examined for ubiquitylation of individual histones. Reactions were performed using 1 μg of recombinant histones (as indicated). I^{125} autoubiquitylated Ring1B/Mel-18 (asterix) product is indicated.

nucleosomal targeting of melPRC1 requires prior phosphorylation of Mel-18. Collectively, these results show that the RING finger protein Mel-18 plays a critical role in recruiting polycomb proteins to chromatin and provide a link between polycomb-mediated gene repression and cell signaling pathways.

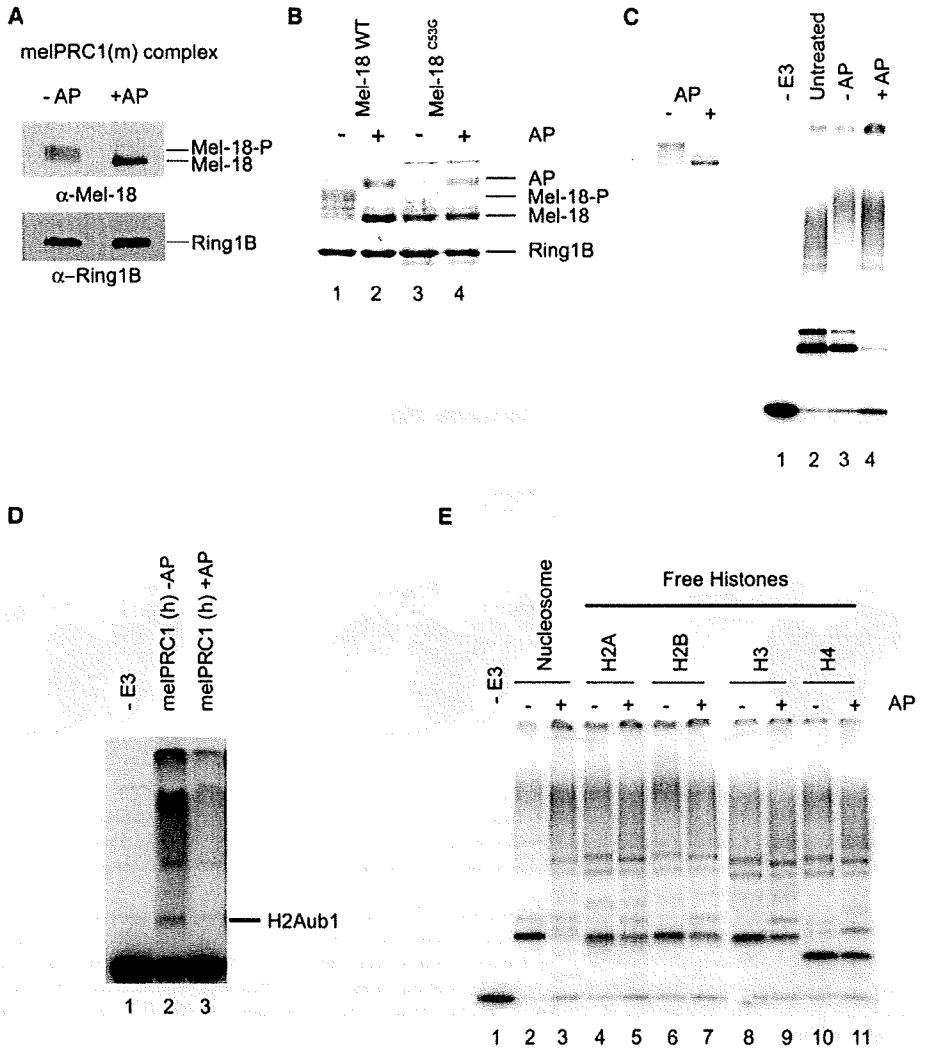

Figure 6. Phosphorylated Form of Mel-18 Directs Ring1B to Chromatin

(A) Mel-18 isolated from ES cells is phosphorylated. Western blot of Mel-18 complex melPRC1 isolated from BM3-3 cells (see Figure S1B). The complex was treated with AP or buffer for 1 hr and immunoblotted for Mel-18 or Ring1B antibody. Phosphorylated and nonphosphorylated forms of Mel-18 are indicated.

(B) Recombinant Ring1B/Mel-18, but not mutant Ring1B/Mel-18^{C53G}, complex is phosphorylated. Purified Ring1B/Mel-18 and Ring1B/Mel-18^{C53G} were treated with AP. AP, Ring1B, and the phosphorylated and nonphosphorylated forms of Mel-18 are indicated.

(C) Dephosphorylation of Mel18 ablates E3 ligase activity on nucleosomes. Left panel, Ring1B/Mel-18 complex treated, or not, with AP. Right panel, AP-treated and -untreated complex was assayed for ubiquitin ligase activity on nucleosome substrate.

(D) Dephosphorylation of the melPRC1 complex purified from 293T cells ablates E3 ligase activity on nucleosomes. AP-treated complex was assayed for ubiquitin ligase activity on nucleosome substrate.

(E) AP-treated Ring1B/Mel-18 retains the ability to ubiquitylate free histones. AP-treated and -untreated complex was assayed for ubiquitin ligase activity on nucleosomes or recombinant histones.

Functional Interchangeability of PRC1-like Complexes

The function of individual PRC1 components in higher organisms is poorly understood. Previous studies demonstrated that while Mel-18 and Bmi1 knockout mice have similar, though not identical, phenotypes (Akasaka et al., 1996, 1997; van der Lugt et al., 1994, 1996), the double knockout mouse embryos exhibit a more profound phenotype (Akasaka et al., 2001). This suggests that while these two proteins have independent functions, they may also exhibit some functional redundancy. This view is supported by our demonstration that Mel-18 can restore repression of *Hox* gene expression to Mel18$^{-/-}$Bmi1$^{-/-}$ ES cells.

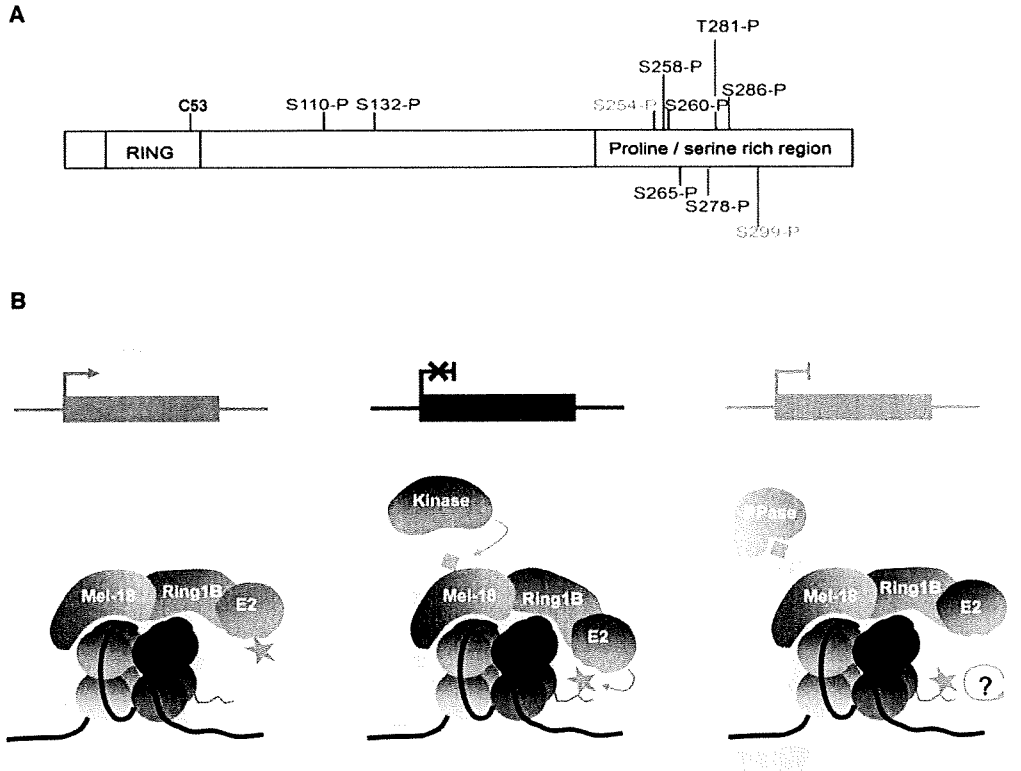

Figure 7. The Mel-18 Polycomb Complex Regulates Gene Expression

(A) Schematic representation of the Mel-18 protein showing the conserved RING domain containing the cysteine at position 53, and the proline/serine rich domain. Amino acid residues that have been identified by mass spectrometry analysis as being phosphorylated are shown. Red amino acids are phosphorylated in Mel-18 and conserved in Bmi1; green amino acids are phosphorylated in Mel-18 but are not conserved in Bmi1. Amino acid S132 was found to be a minor phosphorylated residue.

(B) Schematic diagram representing a model for the regulation of melPRC1 in H2A ubiquitylation. The unphosphorylated melPRC1 complex is proposed to bind chromatin. Phosphorylation of Mel-18 (blue diamond) by a putative Mel-18 kinase then brings about a conformational change, aligning the E2-conjugating enzyme appropriately to allow transfer of the ubiquityl group (orange star) to lysine 119 in the H2A tail. Mel-18 phosphorylation may represent the default state with regulation of the complex conferred by a phosphatase (PPase) that dephosphorylates Mel-18 and thereby derepresses associated target genes. Derepression requires removal of the ubiquityl group from H2A lysine 119 either by an active or passive mechanism (indicated with question mark).

In keeping with this notion, we find that MEL-18 (Mel-18) is part of a multiprotein complex with RING1/2 (Ring1A/B), HPH2a (mPh2), and CBX8 (mPc3), all of which also associate with BMI1 (Bmi1) (Levine et al., 2002; Wang et al., 2004) (Figure S1). However, since MEL-18 and BMI1 components are not found together in the same complex, they probably participate in distinct polycomb repressor complexes (melPRC1 and bmi1PRC1, respectively). This may explain the nonoverlapping functions of Mel-18 and Bmi1 defined in genetic experiments.

Mechanism of H2A Lysine 119 Ubiquitylation

Biochemical analyses of Ring1B/Bmi1 (Cao et al., 2005) and Ring1B/Mel-18 (this study) suggest that the two RING finger proteins synergize to form an active core that is sufficient for the efficient ubiquitylation of H2A lysine 119. The fact that Cao et al. (2005) failed to detect H2A ubiquitylation using Mel-18 in complex with Ring1B may be attributable either to differences in the recombinant Mel-18 protein used in the two studies, for example the levels of phosphorylation at a specific site(s), or alternatively to differences in the assay conditions used.

In both subcomplexes, the Ring1B subunit is essential for ubiquitin transfer. It is generally held that RING finger E3 ligases provide a scaffold, which recruits both the ubiquitin-charged E2 enzyme and the substrate, juxtaposed so that transfer of ubiquitin can occur directly from E2 to substrate (Zheng et al., 2002). Our data suggest that Ring1B performs only the first of these functions, recruitment of the E2-conjugating enzyme. Consequently, mutations in Ring1B that alter the structure of the RING domain or interfere with the recruitment of the E2 abolish E3 function against chromatin or free histone substrates as well as autoubiquitylation. It is of note that we find no significant ubiquitin ligase activity with the Ring1B subunit alone.

On the other hand, a similar mutation (C53G) in the RING domain of Mel-18 abolishes ubiquitylation of nucleosome substrates, but not autoubiquitylation or the ubiquitylation of free histones. This suggests that while Mel-18 is not essential for E3 function per se, it is required to position the E3 ligase for the specific ubiquitylation of H2A lysine 119 in a chromatin context. Furthermore, the failure of the C53G mutant complex to ubiquitylate nucleosomes can be attributed to the fact that this mutant Mel-18 is not phosphorylated (see below). Extrapolating our observations, we suggest that other PSC paralogs, Bmi1, NSPc1, and MBLR, may carry out an equivalent function in targeting the E3 ligase activity of Ring1A/B to H2A lysine 119 in chromatin. The presence of the different PSC paralogs would allow the targeting of different genes by distinct PRC1-like complexes and/or a tight regulation via different cell signaling pathways.

Regulation of Polycomb Complexes by Phosphorylation

Recent studies have begun to identify how cell signaling pathways regulate gene repression by PcG proteins. Phosphorylation has been shown to reduce the HMTase activity of the PRC2 complex (Cha et al., 2005). Similarly, it has been suggested that phosphorylation of Bmi1 by MAPKAP kinase 3pK results in dissociation of bmiPRC1 from chromatin (Voncken et al., 2005). Jak-stat signaling has been shown to downregulate genes encoding PRC1 components, and this is important in transdifferentiation of imaginal disc cells in *D. melanogaster* (Lee et al., 2005). Our results provide a first example in which phosphorylation enhances activity of a polycomb complex, specifically stimulating recognition of the nucleosome substrate and ubiquitylation of H2A lysine 119 by the melPRC1 E3 ligase.

We identified nine phosphoserine and a single phosphothreonine residue in Mel-18. Sequence analysis reveals that these are consensus sites for multiple serine/threonine kinases, including the casein kinase, cyclin-dependent kinase, and MAPK families. A previous study suggested that phosphorylation of Mel-18 can also be mediated by protein kinase C (Fujisaki et al., 2003). While we cannot rule this out, the majority of sites we identified are not a good consensus for this kinase family. The unambiguous identification of the regulatory kinase for melPRC1 awaits further study.

BMI1 can also be phosphorylated, but only at mitosis, correlating with its dissociation from chromatin (Voncken et al., 2005). Although this is functionally distinct from phosphorylation of Mel-18, it is possible that some of the sites of phosphorylation overlap. Two of the phosphoserine residues identified in Mel-18 (serines 254 and 299) are not conserved in Bmi1. Consequently, these sites may be good candidates for mediating unique functions of Mel-18.

Mel-18 is phosphorylated in Sf9 cells only when complexed with Ring1B (Figure 2C). It is of note that the C53G mutation in Mel-18, which abrogates phosphorylation, does not do so by disrupting this complex. As C53 is located in the RING domain of Mel-18, away from the majority of phosphorylation sites and at a residue that is highly conserved in Bmi1 paralogs, we speculate that C53G might alter the conformation of Mel-18 so that recognition by the regulatory kinase(s) is impaired.

How, then, does phosphorylation of Mel-18 impact on the H2A ubiquitylation activity of melPRC1? One possible mechanism is that phosphorylation of Mel-18 is required for the complex to bind to the surface of the nucleosome. Alternatively, phosphorylation may induce a conformational switch in Mel-18 already bound to a nucleosome, positioning Ring1B:E2 for transfer of ubiquitin onto H2A lysine 119. The fact that both phosphorylated and unphosphorylated Mel-18 is found in the chromatin fraction of HeLa cell nuclei perhaps favors the latter hypothesis (Figure S5 and Figure 7B). Structural analyses of phosphorylated and unphosphorylated forms of Mel-18/Bmi1 complexed with Ring1B should provide further insight.

In summary, our data suggest that evolution of the PSC homolog Mel-18 in higher organisms has allowed the acquisition of a distinct mode of regulating H2A ubiquitylation via phosphorylation. Although the biological function of Mel-18 phosphorylation remains to be determined, we envisage two possible models, which are illustrated in Figure 7B. First, a Mel-18 kinase may be regulated so as to repress target genes in response to a specific signal. Second, Mel-18 phosphorylation may be a default state, and regulation of a Mel-18 phosphatase could function to derepress target genes. In future work, identification of Mel-18 kinase/phosphatase activities should shed light on the biological function of Mel-18 phosphorylation in gene regulation by polycomb complexes.

EXPERIMENTAL PROCEDURES

Cell Lines and Derivations

BM3 cells were derived from Mel-18$^{-/+}$/Bmi1$^{-/+}$ heterozygote crosses using standard methods (H.K. and M.E., unpublished data). Generation of BM3 cell lines stably expressing Mel-18-FlagHis are described in the Supplemental Experimental Procedures. BM3 and BM3 transgenic cell lines were grown in DMEM (GIBCO) supplemented with 16% FCS (Autogen Bioclear, Calne, Wiltshire, UK), l-glutamine, nonessential amino acids, 50 IU/ml penicillin/streptomycin, 2-mercaptoethanol (GIBCO), and 1000 units/ml LIF (Chemicon) at 37°C and 5% CO_2.

HeLa cells were grown in DMEM supplemented with 10% FCS l-glutamine and 50 IU/ml penicillin/streptomycin at 37°C and 5% CO_2. Cell-cycle synchronization experiments were carried out as described in the Supplemental Experimental Procedures.

293T cells were cultured at 37°C in a humidified, 5% CO_2 atmosphere in DMEM supplemented to contain 10% FCS, 100 IU/ml penicillin, and 100 μg/ml streptomycin. 293T cells stably expressing human Mel-18-TAP, BMI-1-TAP, or TAP alone were generated as described in the Supplemental Experimental Procedures.

Purification of MEL-18 and BMI1 Complexes by TAP-Tag Purification

Human *MEL-18* and *BMI1* coding sequences were amplified from cDNA and cloned to produce an in-frame TAP tag, generating pGM-MEL-18cTAP or pQBT (BMI1-TAP). pGM-TAP expressing TAP alone was used as a negative control. 293T TAP, 293T, MEL-18TAP, and

293T-ER QBT cells were harvested and protein complexes purified as described in the Supplemental Experimental Procedures.

Purification of Recombinant Mel-18/Ring1B and Mutant Complexes

Full-length mouse Mel-18, Bmi1, and Ring1B were tagged with His_{12} and FLAG or HA and cloned into pDEST8 using the Gateway cloning system (Invitrogen). Mutant Mel-18-FlagHis and Ring1B-FlagHis were generated from the pDEST clones using site-directed mutagenesis kit (Stratagene). Recombinant baculovirus was generated using the Bac-to-Bac baculovirus system (Invitrogen). Wild-type virus vMel-18-HA, or vBmi1-HA, and vRing1B-FlagHis or the reciprocal tagged versions were coinfected in Sf9 insect cells for 60 hr. Complexes were purified as described in the Supplemental Experimental Procedures. Mutant Mel-18-FlagHis and wild-type Ring1B-HA or mutant Ring1B-FlagHis and wild-type Mel-18-HA were coinfected and grown as above. Mutant protein complexes were purified as wild-type complex.

Ubiquitylation Assays

Unless otherwise stated, reactions (25 μl) were performed as described in Mallery et al. (2002) using 300 ng E1 (Boston Biochem), 300 ng UbcH5c (affinity), 1 μg ubiquitin (Sigma), 1 μg purified E3, and 1.5 μg recombinant oligonucleosomes, or 2.5 μg of ES cell chromatin. ^{125}I-labeled products were visualized using the Molecular Dynamics Typhoon Phosphorimager and ImageQuaNT software. Where indicated, complexes were dephosphorylated by treatment with 2 U of AP (Roche 1 U/μl) in phosphatase buffer for 2 hr at 37°C.

Identification of Phosphorylation Sites

Approximately 1 μg of Mel-18 was separated by SDS-PAGE and stained with colloidal Coomassie. Mass spectrometry was carried out as described in the Supplemental Experimental Procedures.

Western Blot Analysis and Antibodies

Antibodies used in western blotting were Mel-18 (Abcam) 1:500, Ring1B (Atsuta et al., 2001) 1:500, Ring1A (Schoorlemmer et al., 1997) 1:500, mPh1 (Miyagishima et al., 2003) 1:10, cyclin A (Santa Cruz) 1:500, cyclin D (Santa Cruz) 1:200, cyclin E (Santa Cruz) 1:100, Lamin (Santa Cruz) 1:2000, and HDAC1 (Santa Cruz) 1:500. Westerns were carried out following protocols provided by the antibody supplier. Secondary antibodies were either sheep anti-mouse IgG HPR linked (GE Healthcare), donkey anti-rabbit Ig HPR linked (GE Healthcare), or donkey anti-goat IgG HRP linked (Santa Cruz). ECL detection (GE Healthcare) was carried out according to the manufacturer's recommendations.

Gene Expression Analysis

RNA from cells was isolated using TRIzol Reagent (Invitrogen) following the manufacturer's instructions. Removal of contaminating DNA using turbo DNase (Ambion) and cDNA synthesis using SuperScript III (Invitrogen) were carried out according to the manufacturer's guidelines. Quantitative real-time PCR was carried out using SYBR Green (Bio-Rad) following the manufacturer's instructions. Data were normalized to the average obtained for two house keeping genes *GAPDH* and *HMBS*. Genes analyzed were *Hoxa1*, *Hoxa5*, *Hoxd4*, *Hoxd8*, and the control gene *Oct-4*. Primer sequences are provided in Table S2. Gene expression levels for the three transgenic cells lines BM3-1, BM3-2, and BM3-3 are represented as a ratio of the parental cell line BM3.

Chromatin Immunoprecipitation

ChIP experiments were carried out as described below. Cells (1×10^8) were fixed with 1% formaldehyde for 10 min at room temperature. The reaction was stopped with a final concentration of 125 mM Glycine. Whole-cell extracts were then sonicated to produce an average DNA fragment size of around 500 bp. Chromatin (150 μg) was used in each immunoprecipitation reaction carried out with either anti-Mel-18 (Santa Cruz), anti-Ring1B (Atsuta et al., 2001), or the appropriate control IgG antibodies overnight at 4°C with rotation. Beads were washed four times with wash buffer 1 and once with final wash buffer. Immunoprecipitated chromatin was eluted from the beads in elution buffer and reverse crosslinked overnight. The precipitated DNA was dissolved in 100 μl of TE. ChIP DNA was analyzed by real-time PCR using SYBR green (Bio-Rad) following the manufacturer's instructions. Enrichment was normalized to input DNA. Primers utilized are shown in Table S3.

Supplemental Data

Supplemental Data include Supplemental Experimental Procedures, seven figures, three tables, and Supplemental References and can be found with this article online at http://www.molecule.org/cgi/content/full/28/1/107/DC1/.

ACKNOWLEDGMENTS

This work was supported by the Medical Research Council (MRC) UK. G.P. and G.N.M. are funded by Cancer Research UK. N.M. is funded by the MRC and by the IRColl for Proteomic technology BBSRC/EPSRC. We thank Dr. Arie Otte for the Ring1A antibody. We are grateful to Dr. T. Akagi (Osaka Bioscience Institute, Osaka, Japan) for providing the pCX4hyg/EcoVR construct. LC-MS/MS was carried at the Taplin Biological Mass Spectrometry Facility (Harvard Medical School, Boston, MA).

Received: March 9, 2007
Revised: June 26, 2007
Accepted: August 3, 2007
Published: October 11, 2007

REFERENCES

Akasaka, T., Kanno, M., Balling, R., Mieza, M.A., Taniguchi, M., and Koseki, H. (1996). A role for mel-18, a Polycomb group-related vertebrate gene, during theanteroposterior specification of the axial skeleton. Development *122*, 1513–1522.

Akasaka, T., Tsuji, K., Kawahira, H., Kanno, M., Harigaya, K., Hu, L., Ebihara, Y., Nakahata, T., Tetsu, O., Taniguchi, M., and Koseki, H. (1997). The role of mel-18, a mammalian Polycomb group gene, during IL-7-dependent proliferation of lymphocyte precursors. Immunity *7*, 135–146.

Akasaka, T., van Lohuizen, M., van der Lugt, N., Mizutani-Koseki, Y., Kanno, M., Taniguchi, M., Vidal, M., Alkema, M., Berns, A., and Koseki, H. (2001). Mice doubly deficient for the Polycomb group genes Mel18 and Bmi1 reveal synergy and requirement for maintenance but not initiation of Hox gene expression. Development *128*, 1587–1597.

Akasaka, T., Takahashi, N., Suzuki, M., Koseki, H., Bodmer, R., and Koga, H. (2002). MBLR, a new RING finger protein resembling mammalian Polycomb gene products, is regulated by cell cycle-dependent phosphorylation. Genes Cells *7*, 835–850.

Atsuta, T., Fujimura, S., Moriya, H., Vidal, M., Akasaka, T., and Koseki, H. (2001). Production of monoclonal antibodies against mammalian Ring1B proteins. Hybridoma *20*, 43–46.

Ben-Saadon, R., Zaaroor, D., Ziv, T., and Ciechanover, A. (2006). The polycomb protein Ring1B generates self atypical mixed ubiquitin chains required for its in vitro histone H2A ligase activity. Mol. Cell *24*, 701–711.

Brunk, B.P., Martin, E.C., and Adler, P.N. (1991). Drosophila genes Posterior Sex Combs and Suppressor two of zeste encode proteins with homology to the murine bmi-1 oncogene. Nature *353*, 351–353.

Brzovic, P.S., Keeffe, J.R., Nishikawa, H., Miyamoto, K., Fox, D., 3rd, Fukuda, M., Ohta, T., and Klevit, R. (2003). Binding and recognition in

the assembly of an active BRCA1/BARD1 ubiquitin-ligase complex. Proc. Natl. Acad. Sci. USA *100*, 5646–5651.

Buchwald, G., van der Stoop, P., Weichenrieder, O., Perrakis, A., van Lohuizen, M., and Sixma, T.K. (2006). Structure and E3-ligase activity of the Ring-Ring complex of polycomb proteins Bmi1 and Ring1b. EMBO J. *25*, 2465–2474.

Cao, R., Wang, L., Wang, H., Xia, L., Erdjument-Bromage, H., Tempst, P., Jones, R.S., and Zhang, Y. (2002). Role of histone H3 lysine 27 methylation in Polycomb-group silencing. Science *298*, 1039–1043.

Cao, R., Tsukada, Y., and Zhang, Y. (2005). Role of Bmi-1 and Ring1A in H2A ubiquitylation and Hox gene silencing. Mol. Cell *20*, 845–854.

Cha, T.L., Zhou, B.P., Xia, W., Wu, Y., Yang, C.C., Chen, C.T., Ping, B., Otte, A.P., and Hung, M.C. (2005). Akt-mediated phosphorylation of EZH2 suppresses methylation of lysine 27 in histone H3. Science *310*, 306–310.

Chen, A., Kleiman, F.E., Manley, J.L., Ouchi, T., and Pan, Z.Q. (2002). Autoubiquitination of the BRCA1*BARD1 RING ubiquitin ligase. J. Biol. Chem. *277*, 22085–22092.

Czermin, B., Melfi, R., McCabe, D., Seitz, V., Imhof, A., and Pirrotta, V. (2002). Drosophila enhancer of Zeste/ESC complexes have a histone H3 methyltransferase activity that marks chromosomal Polycomb sites. Cell *111*, 185–196.

de Napoles, M., Mermoud, J.E., Wakao, R., Tang, Y.A., Endoh, M., Appanah, R., Nesterova, T.B., Silva, J., Otte, A.P., Vidal, M., et al. (2004). Polycomb group proteins Ring1A/B link ubiquitylation of histone H2A to heritable gene silencing and X inactivation. Dev. Cell *7*, 663–676.

Francis, N.J., Saurin, A.J., Shao, Z., and Kingston, R.E. (2001). Reconstitution of a functional core polycomb repressive complex. Mol. Cell *8*, 545–556.

Fritsch, C., Beuchle, D., and Muller, J. (2003). Molecular and genetic analysis of the Polycomb group gene Sex combs extra/Ring in Drosophila. Mech. Dev. *120*, 949–954.

Fujimura, Y., Isono, K., Vidal, M., Endoh, M., Kajita, H., Mizutani-Koseki, Y., Takihara, Y., van Lohuizen, M., Otte, A., Jenuwein, T., et al. (2006). Distinct roles of Polycomb group gene products in transcriptionally repressed and active domains of Hoxb8. Development *133*, 2371–2381.

Fujisaki, S., Ninomiya, Y., Ishihara, H., Miyazaki, M., Kanno, R., Asahara, T., and Kanno, M. (2003). Dimerization of the Polycomb-group protein Mel-18 is regulated by PKC phosphorylation. Biochem. Biophys. Res. Commun. *300*, 135–140.

Gearhart, M.D., Corcoran, C.M., Wamstad, J.A., and Bardwell, V.J. (2006). Polycomb group and SCF ubiquitin ligases are found in a novel BCOR complex that is recruited to BCL6 targets. Mol. Cell. Biol. *26*, 6880–6889.

Hashizume, R., Fukuda, M., Maeda, I., Nishikawa, H., Oyake, D., Yabuki, Y., Ogata, H., and Ohta, T. (2001). The RING heterodimer BRCA1-BARD1 is a ubiquitin ligase inactivated by a breast cancer-derived mutation. J. Biol. Chem. *276*, 14537–14540.

Jorgensen, H.F., Giadrossi, S., Casanova, M., Endoh, M., Koseki, H., Brockdorff, N., and Fisher, A.G. (2006). Stem cells primed for action: polycomb repressive complexes restrain the expression of lineage-specific regulators in embryonic stem cells. Cell Cycle *13*, 1411–1414.

Klymenko, T., Papp, B., Fischle, W., Kocher, T., Schelder, M., Fritsch, C., Wild, B., Wilm, M., and Muller, J. (2006). A Polycomb group protein complex with sequence-specific DNA-binding and selective methyllysine-binding activities. Genes Dev. *20*, 1110–1122.

Kuzmichev, A., Nishioka, K., Erdjument-Bromage, H., Tempst, P., and Reinberg, D. (2002). Histone methyltransferase activity associated with a human multiprotein complex containing the Enhancer of Zeste protein. Genes Dev. *16*, 2893–2905.

Kuzmichev, A., Jenuwein, T., Tempst, P., and Reinberg, D. (2004). Different EZH2-containing complexes target methylation of histone H1 or nucleosomal histone H3. Mol. Cell *14*, 183–193.

Lee, N., Maurange, C., Ringrose, L., and Paro, R. (2005). Suppression of Polycomb group proteins by JNK signalling induces transdetermination in Drosophila imaginal discs. Nature *438*, 234–237.

Levine, S.S., Weiss, A., Erdjument-Bromage, H., Shao, Z., Tempst, P., and Kingston, R.E. (2002). The core of the polycomb repressive complex is compositionally and functionally conserved in flies and humans. Mol. Cell. Biol. *22*, 6070–6078.

Li, Z., Cao, R., Wang, M., Myers, M.P., Zhang, Y., and Xu, R.M. (2006). Structure of a Bmi-1-Ring1B polycomb group ubiquitin ligase complex. J. Biol. Chem. *281*, 20643–20649.

Mallery, D.L., Vandenberg, C.J., and Hiom, K. (2002). Activation of the E3 ligase function of the BRCA1/BARD1 complex by polyubiquitin chains. EMBO J. *21*, 6755–6762.

Miyagishima, H., Isono, K., Fujimura, Y., Iyo, M., Takihara, Y., Masumoto, H., Vidal, M., and Koseki, H. (2003). Dissociation of mammalian Polycomb-group proteins, Ring1B and Rae28/Ph1, from the chromatin correlates with configuration changes of the chromatin in mitotic and meiotic prophase. Histochem. Cell Biol. *120*, 111–119.

Muller, J., Hart, C.M., Francis, N.J., Vargas, M.L., Sengupta, A., Wild, B., Miller, E.L., O'Connor, M.B., Kingston, R.E., and Simon, J.A. (2002). Histone methyltransferase activity of a Drosophila Polycomb group repressor complex. Cell *111*, 197–208.

Ogawa, H., Ishiguro, K., Gaubatz, S., Livingston, D.M., and Nakatani, Y. (2002). A complex with chromatin modifiers that occupies E2F- and Myc-responsive genes in G0 cells. Science *296*, 1132–1136.

Saurin, A.J., Shao, Z., Erdjument-Bromage, H., Tempst, P., and Kingston, R.E. (2001). A Drosophila Polycomb group complex includes Zeste and dTAFII proteins. Nature *412*, 655–660.

Schoorlemmer, J., Marcos-Gutierrez, C., Were, F., Martinez, R., Garcia, E., Satijn, D.P., Otte, A.P., and Vidal, M. (1997). Ring1A is a transcriptional repressor that interacts with the Polycomb-M33 protein and is expressed at rhombomere boundaries in the mouse hindbrain. EMBO J. *16*, 5930–5942.

Schwartz, Y.B., and Pirrotta, V. (2007). Polycomb silencing mechanisms and the management of genomic programmes. Nat. Rev. Genet. *8*, 9–22.

Shao, Z., Raible, F., Mollaaghababa, R., Guyon, J.R., Wu, C.T., Bender, W., and Kingston, R.E. (1999). Stabilization of chromatin structure by PRC1, a Polycomb complex. Cell *98*, 37–46.

Tonkin, E., Hagan, D.M., Li, W., and Strachan, T. (2002). Identification and characterisation of novel mammalian homologues of Drosophila polyhomeotic permits new insights into relationships between members of the polyhomeotic family. Hum. Genet. *111*, 435–442.

van der Lugt, N.M., Domen, J., Linders, K., van Roon, M., Robanus-Maandag, E., te Riele, H., van der Valk, M., Deschamps, J., Sofroniew, M., van Lohuizen, M., et al. (1994). Posterior transformation, neurological abnormalities, and severe hematopoietic defects in mice with a targeted deletion of the bmi-1 proto-oncogene. Genes Dev. *8*, 757–769.

van der Lugt, N.M., Alkema, M., Berns, A., and Deschamps, J. (1996). The Polycomb-group homolog Bmi-1 is a regulator of murine Hox gene expression. Mech. Dev. *58*, 153–164.

van Lohuizen, M., Frasch, M., Wientjens, E., and Berns, A. (1991). Sequence similarity between the mammalian bmi-1 proto-oncogene and the Drosophila regulatory genes Psc and Su(z)2. Nature *353*, 353–355.

Voncken, J.W., Niessen, H., Neufeld, B., Rennefahrt, U., Dahlmans, V., Kubben, N., Holzer, B., Ludwig, S., and Rapp, U.R. (2005). MAPKAP kinase 3pK phosphorylates and regulates chromatin association of the polycomb group protein Bmi1. J. Biol. Chem. *280*, 5178–5187.

Wang, H., Wang, L., Erdjument-Bromage, H., Vidal, M., Tempst, P., Jones, R.S., and Zhang, Y. (2004). Role of histone H2A ubiquitination in Polycomb silencing. Nature *431*, 873–878.

Wei, J., Zhai, L., Xu, J., and Wang, H. (2006). Role of Bmi1 in H2A ubiquitylation and Hox gene silencing. J. Biol. Chem. *281*, 22537–22544.

West, M., and Bonner, W. (1980). Histone 2A, a heteromorphous family of eight protein species. Biochemistry *19*, 3238–3245.

Yamaki, M., Isono, K., Takada, Y., Abe, K., Akasaka, T., Tanzawa, H., and Koseki, H. (2002). The mouse Edr2 (Mph2) gene has two forms of mRNA encoding 90- and 36-kDa polypeptides. Gene *288*, 103–110.

Zheng, N., Schulman, B.A., Song, L., Miller, J.J., Jeffrey, P.D., Wang, P., Chu, C., Koepp, D.M., Elledge, S.J., Pagano, M., et al. (2002). Structure of the Cul1-Rbx1-Skp1-F boxSkp2 SCF ubiquitin ligase complex. Nature *416*, 703–709.

doi:10.1038/nature06397

LETTERS

The SRA protein Np95 mediates epigenetic inheritance by recruiting Dnmt1 to methylated DNA

Jafar Sharif[1,2,3]*, Masahiro Muto[4]*, Shin-ichiro Takebayashi[6]*, Isao Suetake[7], Akihiro Iwamatsu[8], Takaho A. Endo[5], Jun Shinga[4], Yoko Mizutani-Koseki[4], Tetsuro Toyoda[5], Kunihiro Okamura[2], Shoji Tajima[7], Kohzoh Mitsuya[1], Masaki Okano[6] & Haruhiko Koseki[4]

DNA methyltransferase (cytosine-5) 1 (Dnmt1) is the principal enzyme responsible for maintenance of CpG methylation and is essential for the regulation of gene expression, silencing of parasitic DNA elements, genomic imprinting and embryogenesis[1–4]. Dnmt1 is needed in S phase to methylate newly replicated CpGs occurring opposite methylated ones on the mother strand of the DNA, which is essential for the epigenetic inheritance of methylation patterns in the genome. Despite an intrinsic affinity of Dnmt1 for such hemi-methylated DNA[5], the molecular mechanisms that ensure the correct loading of Dnmt1 onto newly replicated DNA *in vivo* are not understood. The Np95 (also known as Uhrf1 and ICBP90) protein binds methylated CpG through its SET and RING finger-associated (SRA) domain[6]. Here we show that localization of mouse Np95 to replicating heterochromatin is dependent on the presence of hemi-methylated DNA. Np95 forms complexes with Dnmt1 and mediates the loading of Dnmt1 to replicating heterochromatic regions. By using Np95-deficient embryonic stem cells and embryos, we show that Np95 is essential *in vivo* to maintain global and local DNA methylation and to repress transcription of retrotransposons and imprinted genes. The link between hemi-methylated DNA, Np95 and Dnmt1 thus establishes key steps of the mechanism for epigenetic inheritance of DNA methylation.

Methylation inheritance is the process of copying pre-existing methylation patterns onto the new DNA strand after DNA replication[7]. Dnmt1 prefers to methylate hemi-methylated CpG regions, which appear after the replication and repair steps, and thus has a dominant role in methylation inheritance[8]. Loading of Dnmt1 onto its targets involves proliferating cell nuclear antigen (Pcna), which promotes Dnmt1 localization to replication foci, but Pcna is not absolutely required in this process[9,10]. Therefore, the molecular mechanisms that load Dnmt1 to the hemi-methylated CpG regions remain largely obscure. Recently, the *Arabidopsis* SRA protein VIM1 has been shown to be involved in recognition of methylated CpG and DNA methylation[11]. A closely related human protein NP95 also binds to methylated promoters through its SRA domain, and mouse Np95 is essential for cell-cycle progression, DNA damage responses and replication of pericentromeric heterochromatin[6,12–14]. Therefore, Np95 is a possible candidate linking Dnmt1 with hemi-methylated DNA in mammals.

To test this possibility, we first examined the localization of Np95 in embryonic stem cells (ESCs) by immunofluorescence analysis. Because Np95 is known to colocalize with replication foci in mid-to-late-S-phase fibroblasts[14], we sorted ESCs into representative cell-cycle stages and then stained them with 4,6-diamidino-2-phenylindole (DAPI), and Np95, Dnmt1 and Pcna antibodies (Fig. 1a). There was an intense accumulation of Np95 at DAPI-dense heterochromatin regions in mid-to-late-S-phase nuclei, but not in the G1 or G2/M phase. We confirmed colocalization of Np95 with Dnmt1 and Pcna in mid-to-late-S-phase ESC nuclei, an observation that prompted us to investigate whether human NP95 forms complexes with DNMT1. *In vivo* biotinylated NP95 was used in a pull-down assay[15] (Supplementary Fig. 1). We tested for the presence of DNMT1 in NP95 complexes by immunoblotting, and found significant quantities (Fig. 1b) of catalytically active NP95-associated DNMT1 (ref. 16, Supplementary Fig. 2). Because DNMT1 interacts with PCNA[9,10], we extended the analysis to PCNA and also found PCNA in the NP95 complexes (Fig. 1b). Taken together, these results indicate that NP95 forms complexes with DNMT1 and PCNA at replicating heterochromatic regions[17], where hemi-methylated DNA is generated and concurrently converted into full-methylated DNA on both strands.

We next examined whether the localization of Np95 is dependent on methylated DNA using various *Dnmt*-deficient ESCs with characteristic DNA methylation profiles. In wild-type ESCs, Np95 exhibited a focal accumulation in replicated heterochromatin in a small fraction of cells (~20%) and a diffuse localization pattern in the rest (Fig. 1c–e). A similar Np95 distribution profile was seen in *Dnmt3a*$^{-/-}$;*Dnmt3b*$^{-/-}$ double-knockout (DKO) ESCs (Fig. 1c–e), which retain considerable global DNA methylation[18]. Np95 was also able to localize to heterochromatin in *Dnmt1*$^{-/-}$ ESCs (Fig. 1c, e), in which global DNA methylation is extensively decreased but not abolished[18,19]. Interestingly, the percentage of *Dnmt1*$^{-/-}$ ESCs showing Np95 heterochromatin accumulation was much higher than in wild-type and 3abDKO ESCs (Fig. 1c). In contrast, Np95 showed a diffuse localization pattern and almost no enrichment in the newly replicated heterochromatin in *Dnmt1*$^{-/-}$;*Dnmt3a*$^{-/-}$;*Dnmt3b*$^{-/-}$ triple knockout (TKO) ESCs (Fig. 1c–e), in which DNA methylation is absent[19]. These findings support the idea that localization of Np95 to replicating heterochromatin is dependent on methylated DNA. To confirm this, we transiently expressed Dnmt3a and Dnmt3b, both of which methylate DNA at pericentric heterochromatin, as either wild-type or catalytically defective mutants in TKO ESCs and examined the heterochromatin localization of Np95 (refs 20 and 21; Fig. 1f and Supplementary Fig. 3). Dnmt3a and Dnmt3b restored the heterochromatin localization of Np95, whereas the catalytically defective mutants did not. These findings indicate that the heterochromatin

[1]Tohoku University Biomedical Engineering Research Organization (TUBERO), 2-1 Seiryo-machi, Aoba-ku, Sendai 980-8575, Japan. [2]Department of Obstetrics and Gynecology, Tohoku University School of Medicine, 1-1 Seiryo-machi, Aoba-ku, Sendai 980-8574, Japan. [3]Department of Chemistry and Biotechnology, Graduate School of Engineering, The University of Tokyo, 7-3-1 Hongo, Bunkyo-ku, Tokyo 113-8656, Japan. [4]RIKEN Research Center for Allergy and Immunology, [5]RIKEN Genomic Sciences Center, 1-7-22 Suehiro, Tsurumi-ku, Yokohama 230-0045, Japan. [6]RIKEN Center for Developmental Biology, 2-2-3 Minatojima-minamimachi, Chuo-ku, Kobe, Hyogo 650-0047, Japan. [7]Institute for Protein Research, Osaka University, 3-2 Yamadaoka, Suita, Osaka 565-0871, Japan. [8]Protein-Research Network, Inc., 1-13-5 Fukuura, Kanazawa-ku, Yokohama 236-0004, Japan. *These authors contributed equally to this work.

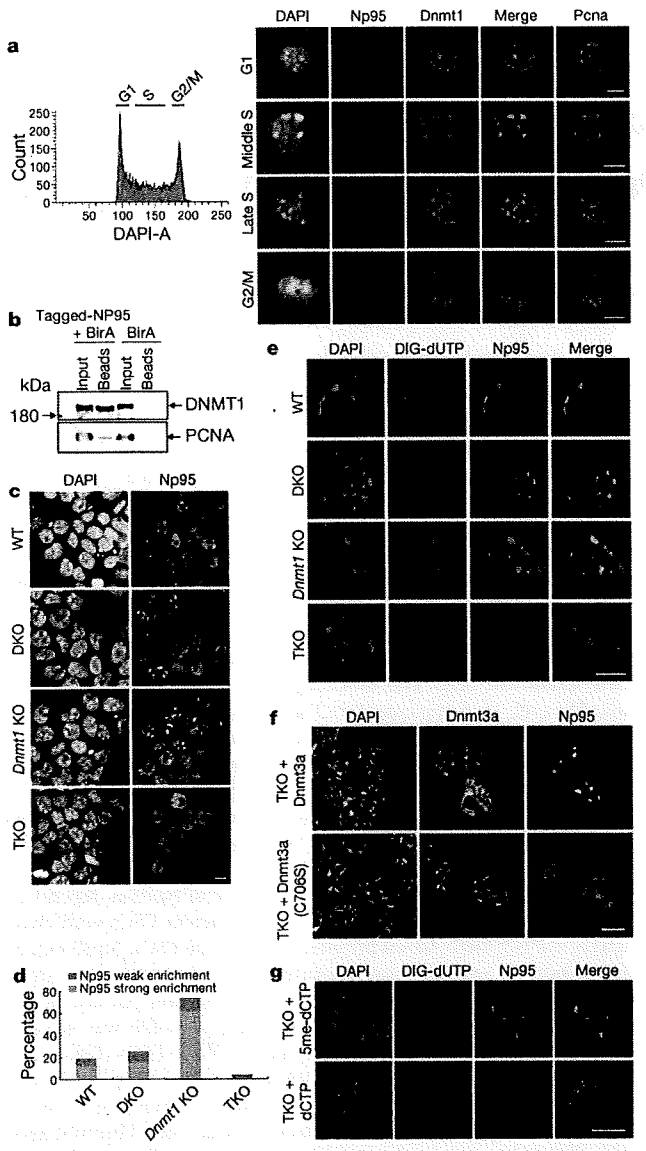

Figure 1 | Local accumulation of Np95 is dependent on hemi-methylated DNA. **a**, Representative subnuclear localization of Np95, Dnmt1 and Pcna in wild-type (WT) ESCs (E14) during cell-cycle progression (right). Merged images for Np95 and Dnmt1 are shown. Profile of DNA content in exponentially growing ESCs is shown (left). DAPI-A is an arbitrary unit that represents fluorescent intensity of cells stained by DAPI. **b**, Association of NP95 with DNMT1 and PCNA in HeLa cell nuclear extracts. HeLa cells transfected with expression vectors for BirA *Escherichia coli* biotin-protein ligase and tagged-NP95 are indicated as 'Tagged-NP95 + BirA', whereas those transfected with BirA alone are labelled 'BirA'. **c**, Immunofluorescence analysis of Np95 in wild-type, *Dnmt3a*$^{-/-}$;*Dnmt3b*$^{-/-}$ DKO, *Dnmt1* knockout (KO) and *Dnmt1*$^{-/-}$;*Dnmt3a*$^{-/-}$;*Dnmt3b*$^{-/-}$ TKO ESCs. **d**, Frequency of cells exhibiting heterochromatic localization of Np95 in respective ESCs. More than three-hundred cells were visually scored for the degree of speckled localization of Np95 for either strong or weak enrichment at the heterochromatic regions. **e**, Nuclear localization of Np95 during replication of the pericentromeric heterochromatin. Replication sites were visualized by the incorporation of digoxigenin-11 (DIG)-dUTP. **f**, Localization of Np95 in TKO ESCs, in which a wild-type or catalytic-defective (C706S) Dnmt3a was transiently expressed. **g**, Localization of Np95 in TKO ESCs, in which methylated or unmethylated dCTP was incorporated simultaneously with DIG-dUTP. Scale bars represent 10 μm.

accumulation of Np95 during S phase is dependent on the DNA methylation mark rather than on the presence of Dnmt3 proteins.

Given that the primary Dnmt1 substrate for methylation inheritance is hemi-methylated DNA, we hypothesized that Np95 primarily recognizes hemi-methylated CpG, which is enriched in newly replicated regions and thus is distributed in the nuclei in a cell-cycle-dependent manner. Consistent with this hypothesis, Np95 accumulated in heterochromatin in most *Dnmt1*$^{-/-}$ ESCs independently of the cell-cycle stage, whereas the heterochromatin enrichment of Np95 was barely detectable in the early S phase of the wild-type cells (Fig. 1c and Supplementary Fig. 4). This difference could be explained by increased hemi-methylated CpG in *Dnmt1*$^{-/-}$ ESCs, as has been seen in *DNMT1*-defective human cancer cells[22], whereas heterochromatic regions are probably symmetrically CpG-methylated in wild-type ESCs in early S phase. We thus examined colocalization of Np95 and hemi-methylated DNA by replication labelling, in which 5-methyl-dCTP is incorporated into the nascent strand of an unmethylated TKO genome[23]. Np95 was prominently accumulated in heterochromatin when 5-methyl-dCTP was incorporated into TKO ESCs (Fig. 1g). These results strongly support a model in which local accumulation of Np95 is dependent on hemi-methylated DNA. Consistent with our observations, the recombinant SRA domain has been shown recently to bind hemi-methylated CpG *in vitro*[24].

We went on to examine the affect of Np95 loss on DNA methylaion[13] (Supplementary Fig. 5). *Np95*$^{-/-}$ embryos show developmental arrest shortly after gastrulation and exhibit early gestational lethality in a similar manner to *Dnmt1*$^{-/-}$ embryos. Genomic DNA isolated from *Np95*$^{-/-}$ and wild-type ESCs or embryos was evaluated for the degree of global and local DNA methylation. *Dnmt1*$^{-/-}$ ESCs were used as a reference in these experiments[18]. The level of global DNA methylation in the absence of Np95 was determined by examining the resistance of the DNA to methylation-sensitive restriction enzymes. Global CpG methylation was reduced substantially in *Np95*$^{-/-}$ ESCs and embryos (Fig. 2a).

To refine our analysis, we next examined CpG methylation levels at heterochromatic domains. Major and minor satellites at pericentromeric and centromeric heterochromatin, respectively, are highly compacted and condensed; this is, at least in part, caused by the high levels of methylated CpG. DNA blot analyses for major and minor satellites revealed extensive hypomethylation in both *Np95*$^{-/-}$ and *Dnmt1*$^{-/-}$ ESCs (Fig. 2b). We further investigated CpG methylation levels by immuofluorescence using a 5-methylcytosine antibody. Intense 5-methylcytosine staining at pericentromeric regions was seen in the mitotic chromosomes and interphase nuclei of wild-type ESCs, but was significantly reduced in *Dnmt1*$^{-/-}$ and was totally abolished in TKO cells (Fig. 2c). In *Np95*$^{-/-}$ ESCs, 5-methylcytosine staining was reduced to a level similar to that in *Dnmt1*$^{-/-}$ ESCs, but was less than levels in TKO cells. The methylation defect in *Np95*$^{-/-}$ cells was complemented by expression of Myc-tagged Np95. Equivalent data were obtained for the major satellite sequences by DNA bot analyses (Supplementary Fig. 6). In summary, CpG methylation in heterochromatic regions is reduced to a similar extent in *Np95*$^{-/-}$ and *Dnmt1*$^{-/-}$ ESCs.

Most CpGs are methylated at retrotransposon-derived elements in euchromatic regions. Loss of DNA methylation by Dnmt1 inactivation results in derepression of silenced retrotransposons[4]. We thus examined DNA methylation at the promoter regions of the intracisternal A particle (IAP) and long interspersed nuclear element 1 (LINE-1) retrotransposons. Hypomethylation of IAP retrotransposons in *Np95*$^{-/-}$ ESCs was demonstrated by DNA blot analysis (Fig. 2d). Moreover, hypomethylation of IAP and LINE-1 elements in *Np95*$^{-/-}$ embryos was confirmed by bisulphite genomic sequencing (Fig. 2e). Prompted by these findings, we further investigated whether Np95 has a role in genomic imprinting, which is mediated by DNA methylation in somatic cells[2]. CpG methylation at the imprinting control regions of imprinted *H19*, *Kcnq1ot1* (also known as *Lit1*)

and *Gtl2* genes was reduced in *Np95*$^{-/-}$ ESCs (Fig. 2e). Taken together, these results implicate Np95 in DNA methylation at both heterochromatin and euchromatin compartments.

We went on to test whether defects in DNA methylation perturb transcriptional repression in *Np95*$^{-/-}$ embryos. Indeed, RNAi-mediated knockdown of Np95 has been reported to increase pericentromeric transcription[14]. Similarly, in our analysis, IAP, LINE-1 and short interspersed nuclear element 1 (SINE-1) retrotransposons were derepressed in *Np95*$^{-/-}$ embryos (Fig. 3a). We also examined whether parent-of-origin-specific expression at imprinted *H19* and *Kcnq1ot1* loci was retained in *Np95*$^{-/-}$ embryos. In the wild-type embryos, maternally derived *H19* and paternally derived *Kcnq1ot1* were exclusively expressed, whereas, in *Np95*$^{-/-}$ embryos, both alleles were expressed (Fig. 3b). This was accompanied by silencing of the adjacent imprinted transcripts within the clusters (*Igf2* and *Cdkn1c*). Therefore, Np95 is essential for transcriptional silencing of heterochromatin and retrotransposons as well as for parent-of-origin-specific expression of imprinted genes through regulation of CpG methylation status. Taken together, Dnmt1-dependent CpG methylation requires its association with Np95, indicating that Np95 is required either to stimulate the catalytic activity or to direct recruitment of Dnmt1 to its DNA targets.

To test the first possibility, we examined the expression and catalytic activity of Dnmt1 in the absence of Np95. Dnmt1 expression and catalytic activity were comparable in wild-type and *Np95*$^{-/-}$ ESCs (Fig. 4a). We also confirmed that expression of both Dnmt3a and Dnmt3b were maintained (Supplementary Fig. 7). We then addressed the second possibility by determining whether Np95 affects Dnmt1 subnuclear localization. Dnmt1 had either a diffuse localization pattern or a focal accumulation in heterochromatin in wild-type ESCs, as shown in previous studies[17], whereas in almost all *Np95*$^{-/-}$ ESCs Dnmt1 had a diffuse localization pattern (Fig. 4b). The wild-type phenotype was restored by introduction of Myc-tagged Np95. In wild-type cells, Dnmt1 accumulated in the replicating pericentromeric heterochromatin regions in mid-S-phase, and partially retained its heterochromatin localization in late S phase. In contrast, no significant enrichment of Dnmt1 in heterochromatin was observed throughout the S phase in *Np95*$^{-/-}$ ESCs (Fig. 4c). These results demonstrate the requirement of Np95 for proper localization of Dnmt1. Because subnuclear localization of Dnmt1 is dependent on pre-existing DNA methylation marks[23,25] and Np95 binds methylated CpG[24], Np95 is shown to link Dnmt1 to methylated DNA.

Our findings extend our understanding of the molecular mechanism that ensures the fidelity and efficacy of DNA methylation. We have identified binding of the SRA-domain protein Np95 to pre-existing methylated CpG, probably in a hemi-methylated state, as an essential process in loading Dnmt1 to hemi-methylated sites where it mediates accurate and sufficient DNA methylation after

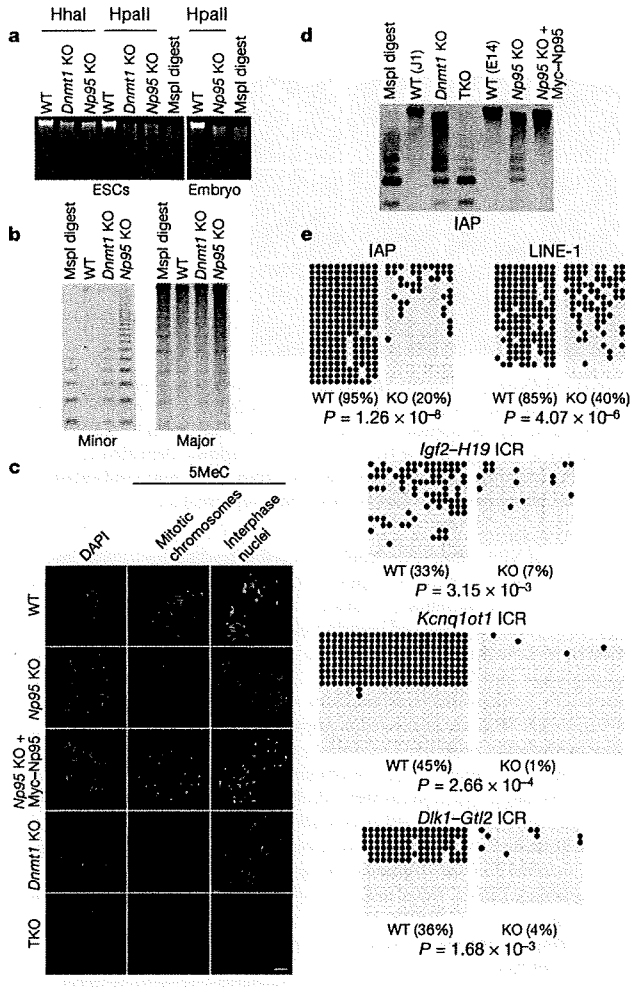

Figure 2 | Impairment of DNA methylation status on *Np95* gene inactivation. **a**, Genome-wide DNA demethylation in *Np95* KO ESCs (left) and embryos (right). **b**, DNA demethylation at the centromeric minor (left) and major (right) satellite repeats. **c**, Anti-5-methylcytosine (5MeC) immunofluorescence in wild-type (WT), *Np95* KO, *Np95* KO + Myc–Np95, *Dnmt1* KO and TKO ESCs in mitotic chromosomes and interphase nuclei. Scale bars represent 10 μm. **d**, DNA demethylation at the IAP retrotransposons. J1 and E14 cells are the parental ESCs for *Dnmt1* and *Np95* KO, respectively. **e**, Extensive demethylation of retrotransposons and imprinting centres in *Np95* KO embryos and ESCs, respectively. Bisulphite sequencing results obtained from E9.5 mouse embryos for IAP and LINE-1, and from ESCs for imprinting control regions (ICRs) of *Igf2–H19*, *Kcnq1ot1* and *Dlk–Gtl2*, are shown. The overall percentage of methylated CpGs is indicated in parentheses. The *P* values indicate the significance of the difference between wild-type and *Np95* KO embryos.

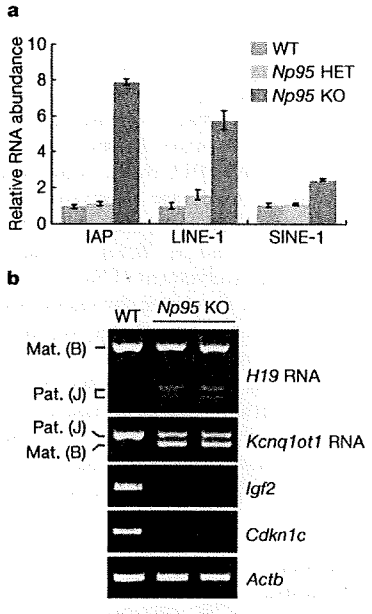

Figure 3 | Misexpression of hypomethylated genes on *Np95* gene inactivation. **a**, Transcriptional derepression of endogenous retrotransposons in *Np95* KO embryos. Error bars represent standard deviation. Total RNA derived from wild-type (WT), heterozygotes (HET) and KO embryos were used. **b**, Disruption of functional imprinting at the two imprinted gene clusters. Monoallelic expression of *H19* (paternal repression) and *Kcnq1ot1* (maternal repression) was lost completely, whereas expression of *Igf2* and *Cdkn1c* was absent in *Np95* KO embryos. B, C57BL/6 strain; J, JF1 strain; Mat., maternal; Pat., paternal; *Actb*, β-actin.

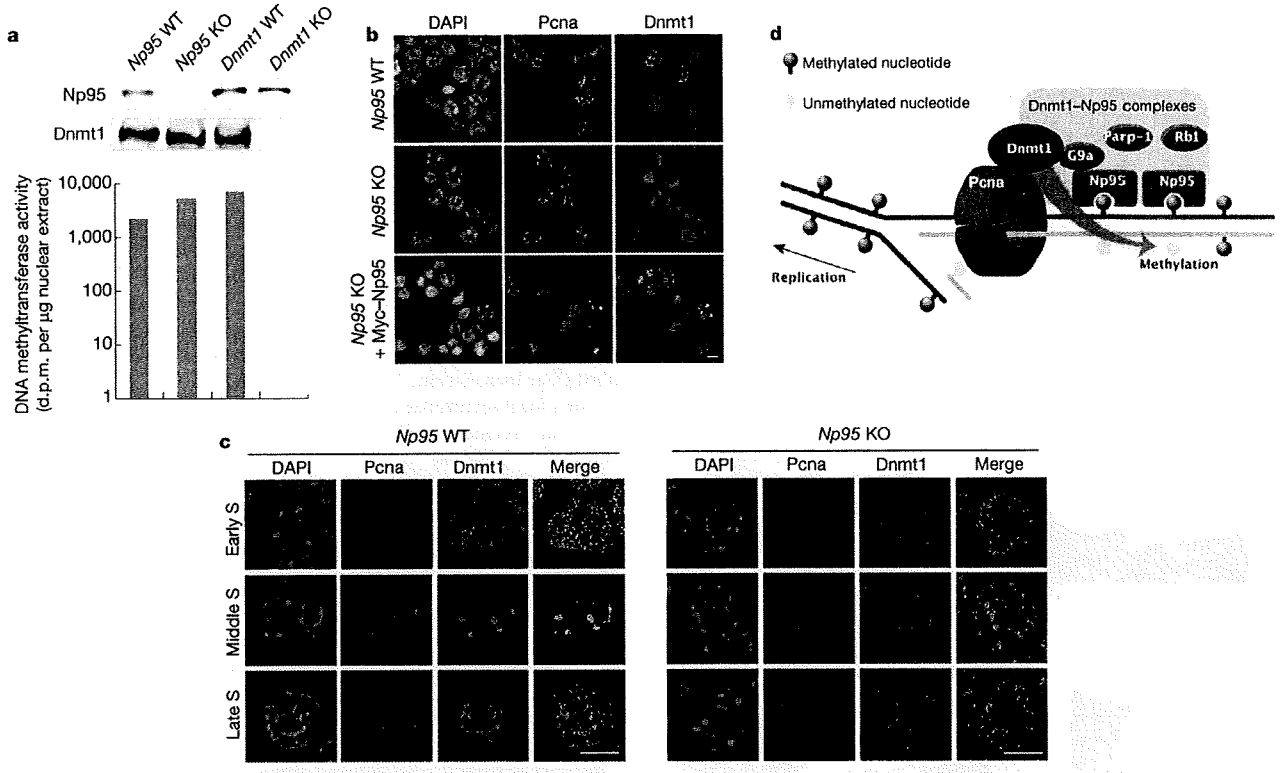

Figure 4 | Np95 is required to target Dnmt1. **a**, DNA methyltransferase activity and the expression of Dnmt1 in *Np95* KO ESCs. d.p.m., decay per minute. **b**, Immunofluorescence analysis of Dnmt1 and Pcna in wild-type, *Np95* KO, and *Np95* KO + Myc–Np95 ESCs. **c**, Nuclear localization of Dnmt1 (green) with Pcna (red) in the early S phase, middle S phase and late S phase of wild-type or *Np95* KO ESCs. The merged images at the right show overlays of Pcna and Dnmt1 staining. The relative contribution of the S-phase stage was not altered in *Np95* KO ESCs (Supplementary Fig. 8). **d**, Schematic representation of molecular actions of Dnmt1–Np95 complexes at the replicating heterochromatic regions identified in this study. Pre-existing and newly synthesized DNA strands are indicated by green and blue lines, respectively. Scale bars represent 10 μm.

replication (Fig. 4d). Consistent with this model, the Np95 SRA domain preferentially binds to hemi-methylated CpG dinucleotides[24]. It is noteworthy that Np95 forms complexes with nuclear proteins involved in DNA repair and chromatin modifications and/or functions[6,14] (Supplementary Tables 1 and 2). The role of Np95 in linking Dnmt1 with DNA repair is probably represented by hypersensitivity to DNA damage observed in the absence of Np95 (ref. 13). Moreover, Np95 complexes share Pcna, Rb1, Parp1 and G9a with Dnmt1 (refs 9 and 26–28; Fig. 1b and Supplementary Table 1). This suggests the involvement of Np95 in sensing not only CpG methylation status but also other chromatin features to guarantee appropriate localization of Dnmt1 (Fig. 4d). Intriguingly, similar methylation defects are seen in cells deficient in Cxxc1, an unmethylated CpG binding protein[29]. This suggests that more proteins recognize CpG methylation status in mediating levels of genomic methylation. Collectively, our findings provide the first evidence that the SRA-domain protein Np95 is required for a hallmark feature of the epigenome, the coordinate regulation of local and global epigenetic features.

METHODS SUMMARY

Immunofluorescence analysis. Detailed procedures for immunostaining and imaging are described in Methods. The following antibodies were used: Np95 rat monoclonal antibody[13], Dnmt1 rabbit polyclonal antibody (Santa Cruz Biotechnology, sc-20701), Pcna mouse monoclonal antibody (Santa Cruz Biotechnology, sc-56), Alexa Fluor-488 goat anti-mouse immunoglobulin G (Molecular Probes, A11017) and Alexa Fluor-555 goat anti-rabbit immunoglobulin G (Molecular Probes, A21430).

Replication labelling. Nucleotide analogues were introduced into cells by a hypotonic shift method as described previously[23,30], with slight modifications as described in Methods.

Pull down of NP95 complexes from HeLa cell extracts. *NP95* complementary DNA was amino-terminally tagged with an oligonucleotide encoding a 23-amino acid biotin-binding domain[15] and was subcloned into pCAGGS. Procedures for cell culture and protein purification are described in Methods.

Mice. *Np95*-deficient mice were generated by using R1 ESCs according to standard protocols, and backcrossed onto a C57BL/6 background for three to six generations[13]. Schematic representations of *Np95* genomic organization and its targeting strategy are illustrated in Supplementary Fig. 1.

DNA methylation analysis. The degree of DNA methylation was assessed by DNA blot hybridization, bisulphite genomic sequencing and 5-methylcytosine immunostaining as described in Methods. Results of bisulphite genomic sequencing were statistically examined as described in Methods.

RNA expression analysis. PCR with reverse transcription analysis was carried out as described in the Methods. Primers used in this study are listed in Supplementary Table 3. Detailed PCR conditions used in this work are available on request.

DNA methyltransferase activity. DNA methyltransferase activity was determined as described previously[16].

Full Methods and any associated references are available in the online version of the paper at www.nature.com/nature.

Received 27 July; accepted 22 October 2007.
Published online 11 November 2007.

1. Li, E., Bestor, T. H. & Jaenisch, R. Targeted mutation of the DNA methyltransferase gene results in embryonic lethality. *Cell* 69, 915–926 (1992).
2. Li, E., Beard, C. & Jaenisch, R. Role for DNA methylation in genomic imprinting. *Nature* 366, 362–365 (1993).
3. Jackson-Grusby, L. *et al.* Loss of genomic methylation causes p53-dependent apoptosis and epigenetic deregulation. *Nature Genet.* 27, 31–39 (2001).
4. Walsh, C. P., Chaillet, J. R. & Bestor, T. H. Transcription of IAP endogenous retroviruses is constrained by cytosine methylation. *Nature Genet.* 20, 116–117 (1998).

5. Fatemi, M., Hermann, A., Pradhan, S. & Jeltsch, A. The activity of the murine DNA methyltransferase Dnmt1 is controlled by interaction of the catalytic domain with the N-terminal part of the enzyme leading to an allosteric activation of the enzyme after binding to methylated DNA. *J. Mol. Biol.* **309**, 1189–1199 (2001).
6. Unoki, M., Nishidate, T. & Nakamura, Y. ICBP90, an E2F-1 target, recruits HDAC1 and binds to methyl-CpG through its SRA domain. *Oncogene* **23**, 7601–7610 (2004).
7. Klose, R. J. & Bird, A. P. Genomic DNA methylation: the mark and its mediators. *Trends Biochem. Sci.* **31**, 89–97 (2006).
8. Goll, M. G. & Bestor, T. H. Eukaryotic cytosine methyltransferases. *Annu. Rev. Biochem.* **74**, 481–514 (2005).
9. Chuang, L. S. *et al.* Human DNA-(cytosine-5) methyltransferase-PCNA complex as a target for p21WAF1. *Science* **277**, 1996–2000 (1997).
10. Spada, F. *et al.* DNMT1 but not its interaction with the replication machinery is required for maintenance of DNA methylation in human cells. *J. Cell Biol.* **176**, 565–571 (2007).
11. Woo, H. R., Pontes, O., Pikaard, C. S. & Richards, E. J. VIM1, a methylcytosine-binding protein required for centromeric heterochromatinization. *Genes Dev.* **21**, 267–277 (2007).
12. Bonapace, I. M. *et al.* Np95 is regulated by E1A during mitotic reactivation of terminally differentiated cells and is essential for S phase entry. *J. Cell Biol.* **157**, 909–914 (2002).
13. Muto, M. *et al.* Targeted disruption of *Np95* gene renders murine embryonic stem cells hypersensitive to DNA damaging agents and DNA replication blocks. *J. Biol. Chem.* **277**, 34549–34555 (2002).
14. Papait, R. *et al.* Np95 is implicated in pericentromeric heterochromatin replication and in major satellite silencing. *Mol. Biol. Cell* **18**, 1098–1106 (2007).
15. de Boer, E. *et al.* Efficient biotinylation and single-step purification of tagged transcription factors in mammalian cells and transgenic mice. *Proc. Natl Acad. Sci. USA* **100**, 7480–7485 (2003).
16. Suetake, I., Miyazaki, J., Murakami, C., Takeshima, H. & Tajima, S. Distinct enzymatic properties of recombinant mouse DNA methyltransferases Dnmt3a and Dnmt3b. *J. Biochem.* **133**, 737–744 (2003).
17. Leonhardt, H., Page, A. W., Weier, H. U. & Bestor, T. H. A targeting sequence directs DNA methyltransferase to sites of DNA replication in mammalian nuclei. *Cell* **71**, 865–873 (1992).
18. Okano, M., Bell, D. W., Haber, D. A. & Li, E. DNA methyltransferases Dnmt3a and Dnmt3b are essential for *de novo* methylation and mammalian development. *Cell* **99**, 247–257 (1999).
19. Tsumura, A. *et al.* Maintenance of self-renewal ability of mouse embryonic stem cells in the absence of DNA methyltransferases Dnmt1, Dnmt3a and Dnmt3b. *Genes Cells* **11**, 805–814 (2006).
20. Bachman, K. E., Rountree, M. R. & Baylin, S. B. Dnmt3a and Dnmt3b are transcriptional repressors that exhibit unique localization properties to heterochromatin. *J. Biol. Chem.* **276**, 32282–32287 (2001).
21. Lin, I. G. *et al.* Murine *de novo* methyltransferase Dnmt3a demonstrates strand asymmetry and site preference in the methylation of DNA *in vitro*. *Mol. Cell. Biol.* **22**, 704–723 (2002).
22. Chen, T. *et al.* Complete inactivation of DNMT1 leads to mitotic catastrophe in human cancer cells. *Nature Genet.* **39**, 391–396 (2007).
23. Takebayashi, S., Tamura, T., Matsuoka, C. & Okano, M. Major and essential role for DNA methylation mark in mouse embryogenesis and stable association of DNMT1 with newly replicated regions. *Mol. Cell. Biol.* **27**, 8243–8258 (2007).
24. Bostick, M. *et al.* UHRF1 plays a role in maintaining DNA methylation in mammalian cells. *Science* **317**, 1760–1764 (2007).
25. Damelin, M. & Bestor, T. H. Biological functions of DNA methyltransferase 1 require its methyltransferase activity. *Mol. Cell. Biol.* **27**, 3891–3899 (2007).
26. Pradhan, S. & Kim, G. D. The retinoblastoma gene product interacts with maintenance human DNA (cytosine-5) methyltransferase and modulates its activity. *EMBO J.* **21**, 779–788 (2002).
27. Reale, A. *et al.* Modulation of DNMT1 activity by ADP-ribose polymers. *Oncogene* **24**, 13–19 (2005).
28. Estève, P. O. *et al.* Direct interaction between DNMT1 and G9a coordinates DNA and histone methylation during replication. *Genes Dev.* **20**, 3089–3103 (2006).
29. Carlone, D. L. *et al.* Reduced genomic cytosine methylation and defective cellular differentiation in embryonic stem cells lacking CpG binding protein. *Mol. Cell. Biol.* **25**, 4881–4891 (2005).
30. Koberna, K. *et al.* Nuclear organization studied with the help of a hypotonic shift: its use permits hydrophilic molecules to enter into living cells. *Chromosoma* **108**, 325–335 (1999).

Supplementary Information is linked to the online version of the paper at www.nature.com/nature.

Acknowledgements This work was supported in part by a grant from the Genome Network Project (to H.K.), by the 'Ground-based Research Program for Space Utilization' promoted by the Japan Space Forum (H.K.) and by a grant-in-aid for Scientific Research on Priority Areas (germ-cell development, reprogramming and epigenetics, to M.O. and K.M.) from the Ministry of Education, Culture, Sports, Science and Technology, Japan. We thank W. Reik, N. Brockdorff, P. Burrows, H. Niwa, H. Sano, J. Strouboulis and M. Vidal for critical reading and reagents.

Author Contributions J. Sharif., K.O. and K.M. performed DNA methylation and gene expression analyses; M.M., Y.M.-K. and H.K. generated, maintained and performed phenotypic analyses of knockout mice; M.M., J. Shinga, and A.I. purified the protein complexes and performed mass spectrometry analyses; S. Takebayashi and M.O. performed immunofluorescence analysis; M.M., I.S. and S. Tajima performed the DNA methylation assay; and T.A.E. and T.T. performed statistical analyses. K.M., M.O. and H.K. designed the study, wrote the paper and contributed equally as co-senior authors. All authors discussed the results and commented on the manuscript.

Author Information Reprints and permissions information is available at www.nature.com/reprints. Correspondence and requests for materials should be addressed to H.K. (koseki@rcai.riken.jp).

METHODS

Immunofluorescence analysis. E14 ESCs grown on culture dishes were collected by trypsinization, fixed with ice-cold 70% ethanol for 30 min, stained with DAPI ($2\,\mu g\,ml^{-1}$), and separated using a cell sorter (Becton Dickinson, FACSDiVa) according to the DNA content. These cells were immunostained as described below.

ESCs were spun onto glass slides, fixed with 4% paraformaldehyde in PBS, permeabilized with 1% Triton X-100 in PBS, incubated in blocking solution (3% BSA, 0.1% Tween 20, 4 × SSC), and then incubated in detection solution containing primary antibodies (1% BSA, 0.1% Tween 20, 4 × SSC). After three washes with 4 × SSC, the samples were incubated in detection solution containing the secondary antibodies. For the Pcna immunostaining, the cells were treated with 0.5% Triton X-100 in CSK buffer (100 mM NaCl, 300 mM sucrose, 10 mM PIPES, pH 6.8, 3 mM $MgCl_2$ and 1 mM EGTA) for 30 s at 4 °C, fixed with paraformaldehyde, and then treated with methanol for 20 min at −20 °C. Images were collected using a Leica DM RA2 fluorescence microscope equipped with a cooled charge-coupled device camera (C4742-95-12ER, Hamamatsu Photonics, Inc.) controlled by a Macintosh G4 computer running the software program IPLab (Signal Analytics). The images were captured at different stage positions and were processed using deconvolution software (Scientific Volume Imaging).

Replication labelling. Fifty micromolar each of DIG-dUTP (Roche Applied Science), dATP, dGTP and dCTP was added to the KHB buffer (10 mM HEPES, pH 7.4, and 30 mM KCl). The mixture was added to cells growing in a 48-well culture dish. After incubation at 37 °C with 5% CO_2 for 30 s, the cells were washed and cultured in normal medium for 10 min to introduce the nucleotides into nascent DNA. DIG-labelled DNA was detected using anti-DIG antibody conjugated with rhodamine. To introduce methylated or unmethylated dCTP into the cell nucleus, 1 mM 5me-dCTP (Roche Applied Science) or dCTP was added with 50 μM DIG-dUTP to KHB buffer. After the hypotonic shift treatment, the cells were cultured for 1 h, and were harvested for immunostaining.

Pull down of NP95 complexes from HeLa cell extracts. Nuclear extracts of HeLa cells transfected with expression vectors for *E. coli BirA* ligase and/or tagged *NP95* were prepared according to standard procedures. Briefly, 6×10^9 cells were harvested by centrifugation at 430*g* and washed twice in cold PBS. The cell pellet was resuspended in 10 mM HEPES (pH 7.9), 1.5 mM $MgCl_2$, 10 mM KCl, 0.5 mM DTT and protease inhibitors (complete, EDTA-free, Roche). The cell suspension was kept on ice for 10 min and was then homogenized with a Wheaton B homogenizer. After centrifugation of the cell lysate for 10 min at 400*g* at 4 °C and, again, at 13,600*g* for 20 min, the nuclear pellets were resuspended in 100 mM KCl Heng buffer (20 mM HEPES, pH 7.9, 100 mM KCl, 20% glycerol, 0.25 mM EDTA and 0.05% NP-40). Next, 2.2 M KCl Heng buffer was added to achieve a final salt concentration of 0.4 M KCl, and nuclei were incubated with rotation for 30 min at 4 °C. The homogenates were ultracentrifuged at 38,000*g* for 1 h at 4 °C, and supernatants were aliquoted, frozen in liquid nitrogen and stored at −80 °C. Nuclear extracts (7.5 mg) were adjusted to 0.1 M KCl Heng buffer with KCl-free Heng buffer, and incubated with paramagnetic streptavidin beads ($25\,\mu l\,mg^{-1}$ protein, Dynabeads M-280), which were pre-blocked with chicken albumin for 1 h at 4 °C on a rotating wheel. The bead–protein complexes were washed six times with 0.1 M KCl Heng buffer, and were resuspended in buffer containing 2.7 M glycerol, 5 mM EDTA, 0.2 mM DTT, 25 mM NaCl, 20 mM Tris-HCl, pH 7.4, and 1% Triton X-100 or SDS sample buffer for DNA methyltransferase assay or MS analysis, respectively.

DNA methylation analysis. DNA blot hybridization was performed to assess the DNA methylation status at the major and minor satellite repeats. Genomic DNA (5 μg) was digested with appropriate restriction enzymes and hybridized with PCR-generated probes. The DNA methylation status at retrotransposons and imprinting centres was determined by use of bisulphite genomic sequencing. Bisulphite treatment of the genomic DNA samples was carried out with the Qiagen EpiTect kit. The amplified fragments were cloned using the TOPO TA cloning kit (Invitrogen), and subsequently sequenced with the BigDye Terminator Cycle Sequencing system (Applied Biosystems). The probes and primers used in this study are listed in Supplementary Table 3. For immunostaining against 5-methylcytosine, ESCs were incubated in a hypotonic solution (0.075 M KCl), fixed in methanol and acetic acid (3:1), and deposited onto a glass slide. After air-drying, slides were irradiated with ultraviolet light for 8 h under a germicidal lamp. Detection of 5-methylcytosine was carried out according to standard immunostaining protocols.

Statistical methods. The non-parametric Mann-Whitney *U*-test was used to analyse the significance of the differences in DNA methylation status between wild-type and $Np95^{-/-}$ embryos or ESCs. A non-parametric method was adopted because the number of methylated nucleotides did not fit a gaussian distribution. The *P* values were calculated using our in-house computer program. To perform statistical tests on imprinted genes, we slightly modified the method because we could not formally distinguish maternal and paternal alleles in these experiments. We therefore hypothesized that genomic sequences with more methylated nucleotides than the median number corresponded to imprinted genes, and performed the Mann-Whitney *U*-test between arbitrarily determined imprinted alleles of wild type and knockout.

RNA expression analysis. Fluorescence real-time PCR analysis was performed on a LightCycler instrument using the SYBR Green detection system according to the protocol provided by the manufacturer (Roche). Each experiment was conducted independently in triplicate to generate a mean and standard deviation. Data were normalized to the level of β-actin gene expression in each individual sample. Monoallelic expression of *H19* (paternal repression) and *Kcnq1ot1* (maternal repression) RNA was investigated using single nucleotide polymorphisms that distinguish the alleles from JF1 and C57BL/6 strains. Total RNA was collected from the offspring of a C57BL/6 × (C57BL/6 × JF1) cross in which the JF1 distal chromosome 7 was paternally inherited. Amplified fragments that included the single nucleotide polymorphisms were analysed by use of restriction-fragment length polymorphisms.

nature
cell biology

Ring1-mediated ubiquitination of H2A restrains poised RNA polymerase II at bivalent genes in mouse ES cells

Julie K. Stock[1*], Sara Giadrossi[2*], Miguel Casanova[3], Emily Brookes[1], Miguel Vidal[4], Haruhiko Koseki[5], Neil Brockdorff[3], Amanda G. Fisher[2,6] and Ana Pombo[1,6]

Changes in phosphorylation of the carboxy-terminal domain (CTD) of RNA polymerase II (RNAP) are associated with transcription initiation, elongation and termination[1–3]. Sites of active transcription are generally characterized by hyperphosphorylated RNAP, particularly at Ser 2 residues, whereas inactive or poised genes may lack RNAP or may bind Ser 5-phosphorylated RNAP at promoter proximal regions. Recent studies have demonstrated that silent developmental regulator genes have an unusual histone modification profile in ES cells, being simultaneously marked with Polycomb repressor-mediated histone H3K27 methylation, and marks normally associated with gene activity[4,5]. Contrary to the prevailing view, we show here that this important subset of developmental regulator genes, termed bivalent genes, assemble RNAP complexes phosphorylated on Ser 5 and are transcribed at low levels. We provide evidence that this poised RNAP configuration is enforced by Polycomb Repressor Complex (PRC)-mediated ubiquitination of H2A, as conditional deletion of Ring1A and Ring1B leads to the sequential loss of ubiquitination of H2A, release of poised RNAP, and subsequent gene de-repression. These observations provide an insight into the molecular mechanisms that allow ES cells to self-renew and yet retain the ability to generate multiple lineage outcomes.

Recent studies have shown that Polycomb proteins are required to silence an important subset of developmental regulator genes in both human and mouse embryonic stem (ES) cells, to ensure that expression occurs only at later stages of ontogeny or upon ES cell differentiation[6–8]. Genome-wide[5] and candidate-based chromatin studies[4] suggest that these genes are enriched for histone modifications associated both with gene activity (such as acetylated histone H3 and trimethylated H3K4) and with PRC2-mediated repression (such as methylated H3K27). Collectively, these reports have encouraged a view that key genes, which are either silent or not productively expressed in ES cells, are poised for future expression (reviewed in ref. 9). Although previous genome-based surveys showed little or no enrichment of RNAP at bivalent genes in ES cells[8] or embryonal cells[10–12], the presence of high levels of promoter acetylation and H3K4me3 prompted us to re-examine this issue.

RNAP is subject to complex phosphorylation of the CTD heptad consensus repeat sequence Tyr[1]-Ser[2]-Pro[3]-Thr[4]-Ser[5]-Pro[6]-Ser[7] (refs 1–3, 13), and binding of Ser 5-phosphorylated RNAP (Ser 5P) has been detected at the promoters of inducible genes prior to their activation[14–16]. Using a modified chromatin immunoprecipitation (ChIP) approach, optimized for use with IgM or IgG antibodies, we examined Ser 5P (4H8), Ser 2P (H5) or total RNAP (H224) binding to the promoter and coding regions of a panel of so-called 'bivalent' genes in ES cells (Fig. 1a). As anticipated, genes that are expressed at high levels in ES cells, such as *β-actin*, *Oct4* and *Sox2*, contained appreciable levels of Ser 5P, Ser 2P and total RNAP. Surprisingly, Ser 5P was detected at the promoter and coding regions of many bivalent genes tested (8 out of 9 genes tested), but was absent from silent genes that lack bivalent chromatin (*Gata1*, *Myf5*, λ5) and have been shown to be unresponsive to withdrawal of PRC1 and 2 (refs 4, 7). Binding of Ser 5P to the promoters of bivalent genes was confirmed in three independent ES cell lines, but was not seen in trophoblast stem (TS) cells (see Supplementary Information, Fig. S1a), a closely related stem cell population with a far more restricted developmental potential. In TS cells, *Cdx2*, *Flk1* and *Gata4* promoters bound RNAP (detected by 8WG16; data not shown), consistent with expression of these genes in trophectoderm tissues. In ES cells, binding of Ser 2P, a form of RNAP associated with elongation and recruitment of the RNA processing machinery[2], was not enriched at any of the bivalent genes analysed but instead, was detected within the coding (or promoter) regions of expressed *β-actin*, *Oct4* and *Sox2* genes (Fig. 1a). Collectively, these results show that RNAP is present at bivalent genes in pluripotent ES cells and is preferentially phosphorylated at Ser 5, but not at Ser 2.

The specificity of antibodies for total RNAP, Ser 2P and Ser 5P has been extensively characterized previously[17], but was confirmed using ES cell extracts prepared in the presence of phosphatase inhibitors and

[1]Nuclear Organisation, [2]Lymphocyte Development and [3]Developmental Epigenetics Groups, MRC Clinical Sciences Centre, Imperial College School of Medicine, Hammersmith Hospital Campus, Du Cane Road, London W12 0NN, UK. [4]Department of Developmental and Cell Biology, Centro de Investigaciones Biológicas, CSIC, Madrid, Spain. [5]Department of Developmental Genetics, RIKEN Research Center for Allergy and Immunology, RIKEN Yokohama Institute, Yokohama, Japan. [6]Correspondence should be addressed to: A.P. or A.G.F (e-mail: ana.pombo@csc.mrc.ac.uk; amanda.fisher@csc.mrc.ac.uk)
*These authors contributed equally to this work.

Received 24 July 2007; accepted 29 October 2007; published online 25 November 2007; DOI: 10.1038/ncb1663

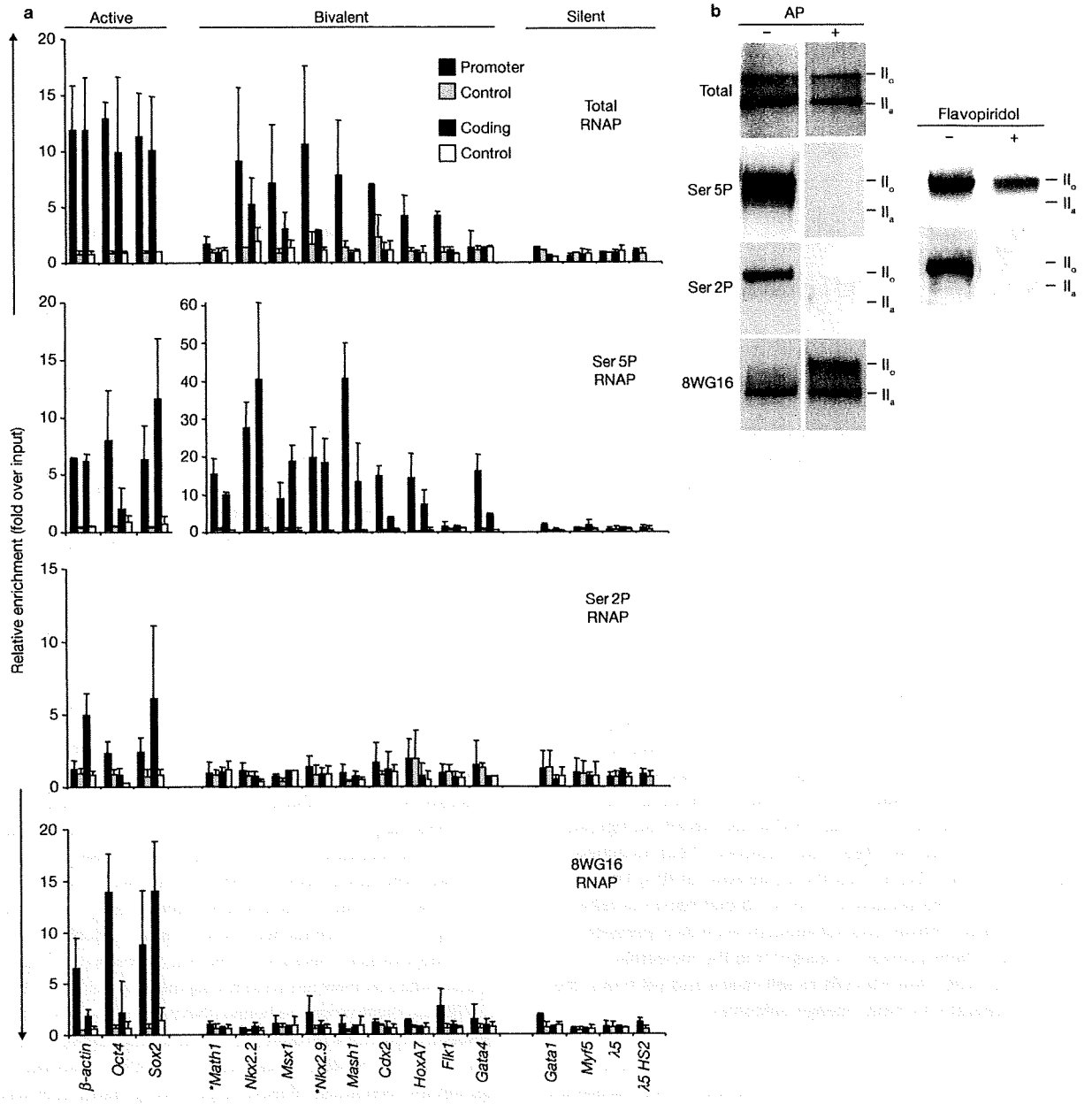

Figure 1 Poised RNAP phosphorylated on Ser 5 marks bivalent genes in ES cells. **(a)** Abundance of different phosphorylated forms of RNAPII at active, bivalent and silent genes in murine ES-OS25 cells assessed by ChIP and qPCR at promoter (blue bars) and coding regions (red bars). Bivalent genes important for subsequent neural specification (*Math1*, *Nkx2.2*, *Msx1*, *Nkx2.9* and *Mash1*), or for extra-embryonic (*Cdx2*), mesodermal (*HoxA7*, *Flk1*) and endodermal (*Gata4*) differentiation are shown. Promoter primers are positioned within –400 base pairs (bp) of transcription start sites, except for *Sox2* (–670 bp). Coding region primers are positioned +2 to +4 kb from start sites, except for *Sox2* (+617 bp). Additional sites in the coding region of several genes consistently showed the presence of RNAP (8 sites in *Nkx2.2* and *Gata4*, 4 in *Msx1*, 3 in *Cdx2*, and 2 in *Mash1* and *Flk1*). * indicates small genes of <2 kb. Enrichment is expressed relative to input DNA using the same amount of DNA in the PCR. Background levels (mean enrichment from control antibodies and beads alone) at promoter and coding regions are shown as pale blue or white bars, respectively. Mean and standard deviations are presented from 3–5 independent experiments, except for total RNAP (two independent experiments). **(b)** Reactivity of different RNAP antibodies against hyper- (II_o) and hypophosphorylated (II_a) forms of the largest subunit of RNAP, RPB1, was assessed by western blotting using whole-cell extracts from ES-OS25 cells treated ±10 μM flavopiridol. SDS–PAGE resolves RPB1 into II_o and II_a forms (also see Supplementary Information, Fig. S7a). Both forms are detected by an antibody against the amino-terminus (H224) that binds independently of phosphorylation. An antibody against Ser 5P CTD peptide (4H8) recognizes the II_o and intermediately phosphorylated bands and has low sensitivity to flavopiridol. Ser 2P RNAP is recognized by H5, which detects only the II_o band and is highly sensitive to flavopiridol. Both 4H8 and H5 reactivities are dependent on phosphorylated epitopes, as shown by treatment of western blot membranes with alkaline phosphatase (AP). An antibody against unphosphorylated CTD (8WG16) detects II_a and intermediately phosphorylated bands, but not highly phosphorylated II_o; AP treatment allows reactivity with II_o.

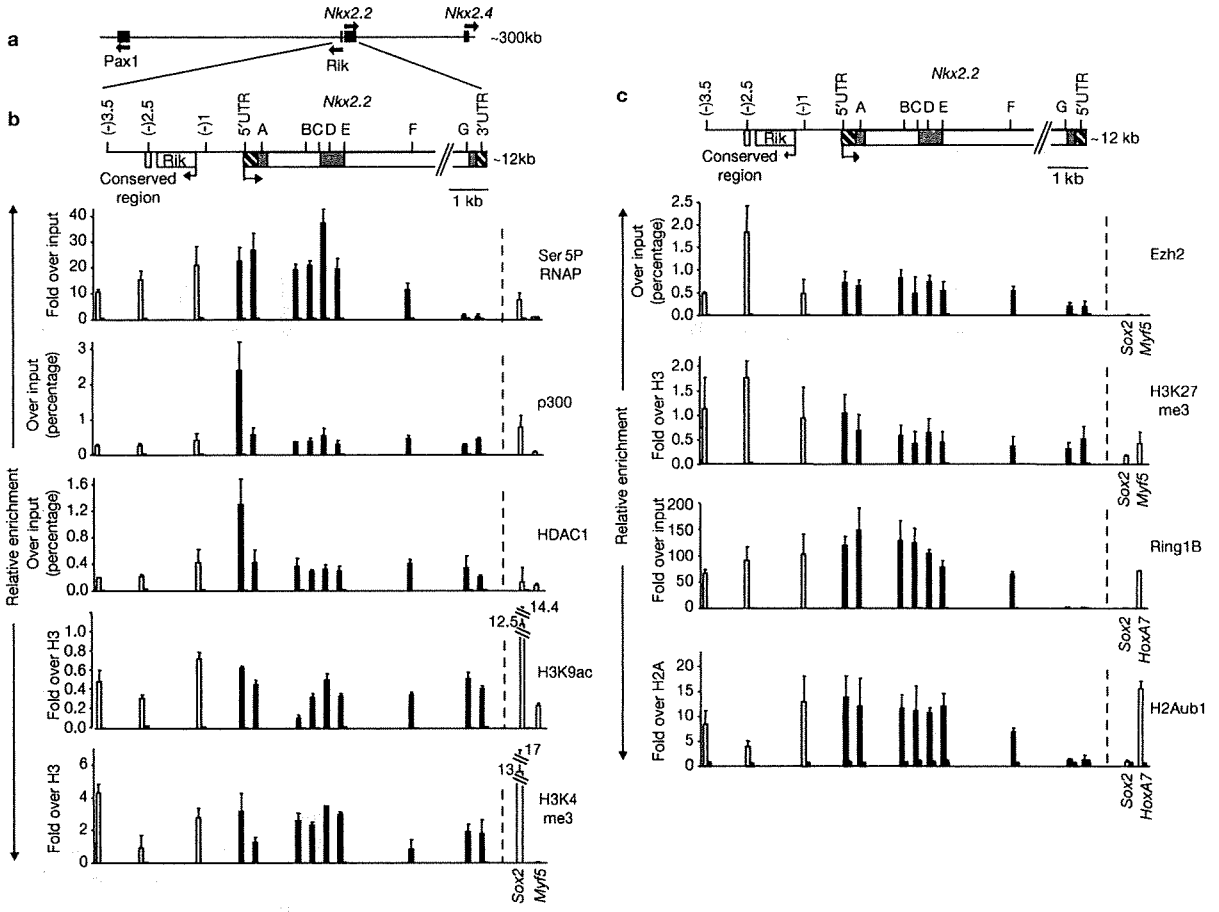

Figure 2 Mapping the binding of transcription machinery and Polycomb repressor components at bivalent chromatin domains in the *Nkx2.2* locus in ES cells. **(a)** Diagram illustrating the genomic context of *Nkx2.2* on mouse chromosome 2. *Nkx2.2* is within a gene-poor region (Ensembl v37, Feb 2006) but is flanked by three genes, *Nkx2.4*, *Pax1* and a gene of unknown function (Rik; *6430503K07Rik*), all of which are silent in ES cells. Arrows indicate direction of transcription. **(b)** ChIP analysis of a 12 kb region of *Nkx2.2* that spans −3.5 kb (upstream of transcription start site; arrow), a conserved region at −2.5 kb (light grey box), and the entire coding region of 8.7 kb containing three exons (dark grey boxes) and untranslated regions (striped boxes). The position of primer pairs used for ChIP analyses is indicated by name or letter. Ser 5P RNAP, p300, HDAC1, H3K9ac and H3K4me3 occupancy across the *Nkx2.2* gene locus was assessed in ES-OS25 cells using ChIP and qPCR. **(c)** Binding of PRC2 and PRC1 components, Ezh2 and Ring1B, and associated histone modifications, H3K27me3 and H2Aub1, across the *Nkx2.2* gene locus. **(b,c)** Enrichment is shown relative to input DNA using the same amount of DNA in the PCR (for Ser 5P, Ring1B, H2Aub1), or relative to total input DNA (for p300, HDAC1, H3K9ac, H3K4me3, H3K27me3, Ezh2), according to the ChIP protocol used to optimize detection. Histone modifications are normalized to unmodified core histones (H3 or H2A). Active (*Sox2*) and silent (*Myf5*) genes were used as controls. *HoxA7*, a known PRC1 target, was used as a positive control for Ring1B and H2Aub1. Background levels, mean enrichment from control antibodies and beads alone (for Ser 5P, Ring1B, H2Aub1), or enrichment from control antibody (for p300, HDAC1, H3K9ac, H3K4me3, Ezh2, H3K27me3) are presented (black bars) next to each data point, and were generally low or negligible. Mean and standard deviations are presented from three independent experiments.

separated by SDS–PAGE to resolve hypo- (II_a) and hyperphosphorylated (II_o) RNAP forms (Fig. 1b). As shown, 4H8 (Ser 5P) and H5 (Ser 2P) antibodies detected II_o and this reactivity was abolished by pre-treatment of transferred proteins with alkaline phosphatase. H224 (used for total RNAP) detects II_a and II_o similarly, whereas antibody 8WG16, a reagent used previously for genome-wide ChIP studies[8,11], recognises predominantly II_a and some intermediately phosphorylated forms[17]. In our ChIP assay, RNAP at bivalent genes was weakly detected by 8WG16 (Fig. 1a). Binding of 8WG16 to the II_o form was demonstrated in western blots following dephosphorylation of the transferred proteins, consistent with phosphorylation obscuring 8WG16 binding (Fig. 1b). The specificity of H5 and 4H8 for Ser 2P and Ser 5P, respectively, was validated using flavopiridol, a potent inhibitor of CDK9, an enzyme that phosphorylates Ser 2 residues, but a weak inhibitor of CDK7, which targets Ser 5 (ref. 18). As predicted, 4H8 detected phosphorylated forms that were unaffected by flavopiridol treatment (Ser 5P), whereas H5 recognition of Ser 2P was abolished (Fig. 1b; see Supplementary Information, Fig. S1b).

To investigate the distribution of Ser 5P at bivalent loci relative to other transcriptional components and chromatin markers, we used ChIP approaches to examine sites spanning the entire *Nkx2.2* locus on chromosome 2 (Fig. 2). *Nkx2.2* is normally expressed by ventral progenitors of the central nervous system in response to high levels of Shh–Gli signalling[19,20], is silent in ES cells, and was previously shown to be up-regulated in ES cells deficient in H3K27 methylation[4]. Ser 5P was detected

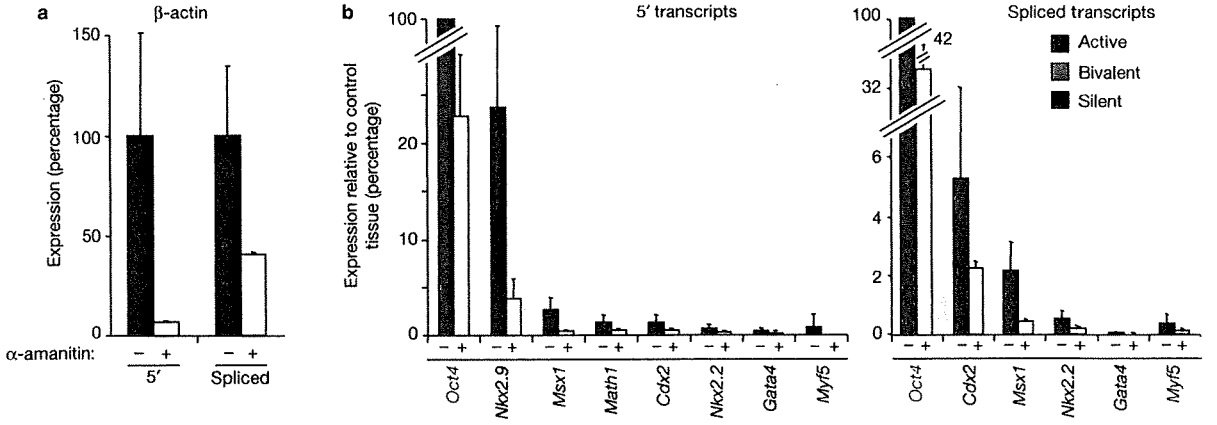

Figure 3 Bivalent genes are transcribed at low level in ES cells. RNA levels were measured by quantitative RT-PCR using ES cells incubated in the absence or presence of α-amanitin (75 μg ml^{-1} for 7 h, to block RNAPII transcription; negative control, open bars). 5′ primers amplifying transcripts spanning the exon 1 and intron 1 junction were used to detect primary transcripts and spliced transcripts were detected using primers located at the exon 1 and exon 2 junction. (**a**) As shown for *β-actin*, treatment with α-amanitin reduced primary transcripts by 93% and spliced transcripts by 60%, consistent with a stable pool of *β-actin* mRNA in ES cells. (**b**) Transcripts derived from genes that are active (green), silent (red) and bivalent (orange) in ES cells were detected using appropriately positioned primers to assess primary and spliced transcripts. Low levels of 5′ and spliced transcripts were detected for all bivalent genes tested, and these were sensitive to inhibition by α-amanitin. These findings indicate that RNAP initiates and elongates at bivalent genes. The results obtained from three independent experiments were normalized to house-keeping genes and values expressed relative to control tissues: embryonic (E15) head (for *Nkx2.9*, *Math1*, *Nkx2.2*, *Msx1*), adult heart (*Gata4*), TS cells (*Cdx2*), C2C12 cells (*Myf5*) and ES-OS25 cells (*Oct4*).

upstream (0–3.5 kb) of the coding region of *Nkx2.2* and within the gene (peak enrichment in the first and second exons), but little binding was detected at downstream regions (exon 3 and 3′UTR, 8 kb from the promoter; Fig. 2b; see Supplementary Information Fig. S1c for an accurate estimate for the resolution of the ChIP approach used here). Interestingly, HDAC1 and p300, two other components of the transcription machinery, also bound at the silent *Nkx2.2* locus in ES cells, with a prominent peak in the 5′UTR. Co-binding of HDAC1 and p300 at promoters of many other bivalent genes was also observed (data not shown). Conventional markers of active euchromatin, including histone H3K9ac and H3K4me3, were enriched throughout *Nkx2.2*, with prominent peaks at −3.5 kb, at the promoter region (−1 to 5′UTR) and within exon 2 (Fig. 2b). The abundance of Ser 5P, p300, HDAC1 and active chromatin marks detected within upstream regions (−3.5 to −1 kb; Fig. 2b) could reflect priming of a RIKEN gene of unknown function that is not expressed in ES cells (data not shown). Histone H3K27me3 and Ezh2, the HMTase responsible for the catalytic activity of PRC2 (refs 21,22), were present throughout *Nkx2.2*, being particularly enriched in the upstream (−2.5 kb) domain (Fig. 2c). Ring1B, a component of PRC1 that catalyses mono-ubiquitination of histone H2A at lysine 119 (H2Aub1)[23,24], was enriched throughout the locus and binding peaked at the first and second exons, similarly to RNAP (Fig. 2c). Consistent with these findings, ChIP analysis for H2Aub1 showed enrichment of this modified histone in the upstream and 5′ coding regions of the *Nkx2.2* gene.

The specificity of H2Aub1 ChIP was verified using control genes that are targets for PRC1-mediated modification in ES cells (*HoxA7*; ref. 25) or that are not targets (*Sox2*; Fig. 2c), and using Ring1B-deficient ES cells (see Supplementary Information, Fig. S2a and below). As expected, Ring1B and H2Aub1 were found at all bivalent genes tested[6] (see Supplementary Information, Fig. S2b). These data show that Ser 5P, HDAC1 and p300 co-locate with PRC1- and PRC2-components at the promoter region of the *Nkx2.2* gene when it is silent in ES cells. Ser 5P is seen to extend into the 5′ coding regions of *Nkx2.2* (exons 1 and 2) where active (H3K9ac, H3K4me3) and repressive (H3K27me3, H2Aub1) histone modifications are also abundant. To confirm that these characteristics are shared by other 'bivalent' loci in ES cells, ChIP analysis was also used to profile the *Msx1* locus on chromosome 5 (see Supplementary Information, Fig. S3). As observed for *Nkx2.2*, high levels of Ser 5P decorate the 5′ regulatory regions of *Msx1* and extend into the coding region of the gene (up to 3 kb). Binding of the transcriptional machinery and distribution of histone modifications were also similar to that previously shown for *Nkx2.2* (see Supplementary Information, Fig. S3).

To directly assess whether RNAP that is present at bivalent genes is transcriptionally active, the production of 5′ and spliced transcripts in ES cells was measured using RT-PCR (Fig. 3). Relative to productively expressed genes such as *β-actin* and *Oct4*, low levels of 5′ and spliced transcripts corresponding to many bivalent genes (*Nkx2.9*, *Gata4*, *Msx1*, *Math1*, *Cdx2*, *Nkx2.2*) were detected in ES cells and were sensitive to the RNAP inhibitor α-amanitin (Fig. 3b). Consistent with recent observations in human cells[12], these results confirm that many bivalent loci are transcribed at low levels in mouse ES cells. Although RNAP levels are comparable to productively expressed genes, the low levels of 5′ transcripts detected suggests either that elongation is inefficient at bivalent genes, or that transcripts are rapidly degraded. This situation contrasts with overt transcription, where RNAP assumes a configuration that is typical of expressed genes. For example, *Gata4*, a gene that is bivalent in ES cells but abundantly expressed in testes, heart and primitive endoderm, showed high levels of Ser 2P (throughout the coding region) and 8WG16 binding (at the promoter) in XEN cells derived from the primitive endoderm (see Supplementary Information, Fig. S4).

Previous studies have demonstrated that bivalent genes are derepressed in ES cell lines homozygous for a null mutation in the PRC2 Polycomb repressor protein Eed[4,6,7]. The PRC1 complex is thought to function downstream of PRC2 (refs 21, 22, 26), and recent studies

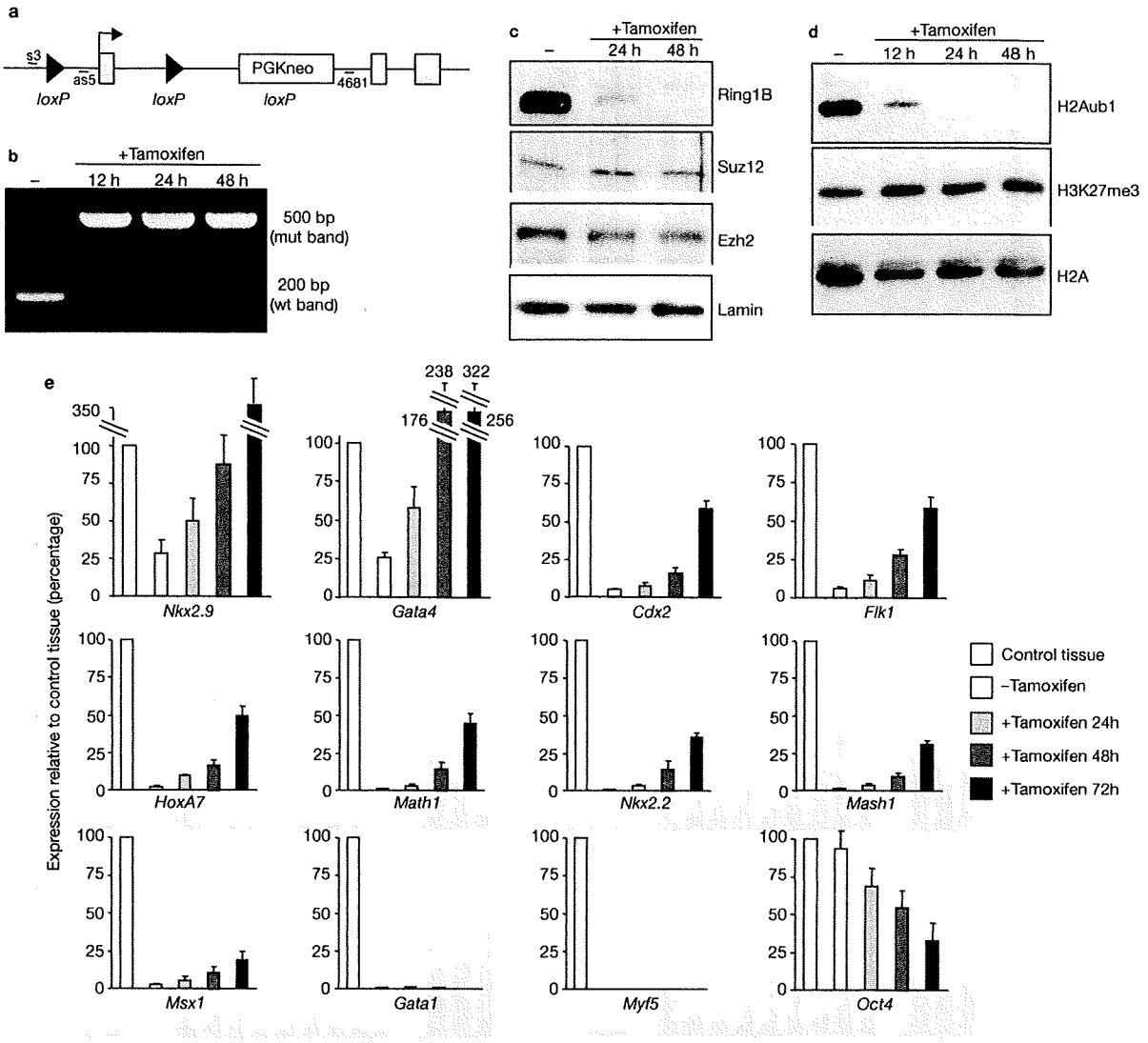

Figure 4 Conditional removal of Ring1B results in a rapid decline in global levels of mono-ubiquitinated H2A and selective de-repression of bivalent genes in ES cells. (**a**) Schematic representation of the *Ring1B* conditional allele. s3, as5 and 4681 are the annealing sites for primers used to check efficient deletion of the *Ring1B* gene in ES-ERT2 cells. (**b**) ES-ERT2 cells containing the *Ring1B* conditional allele were cultured in the presence of 800 nM tamoxifen for 0–48 h. Genomic DNA was extracted and analysed by PCR for the presence of wild-type (wt) and deleted (mut) *Ring1B* alleles. (**c**) Western blot analysis of nuclear extracts of ES-ERT2 cells cultured with 800 nM tamoxifen for 0–48 h, using anti-Ring1B, anti-Suz12, anti-Ezh2, and anti-Lamin (loading control) antibodies. Full-length blot scans are presented in Supplementary Information, Fig. S7b. (**d**) Western blot of acid-extracted histones from ES-ERT2 cells cultured with 800 nM tamoxifen for 0–48 h, using anti-H2Aub1, anti-H3K27me3 and anti-H2A (loading control) antibodies. Full-length blot scans are presented in Supplementary Information, Fig. S7c. (**e**) Kinetics of gene expression in ES-ERT2 cells following tamoxifen treatment. Gene expression was assessed by quantitative RT-PCR. Mean and standard deviation from more than three experiments are represented relative to housekeeping genes and expressed relative to control tissues: embryonic (E15) heads (*Nkx2.9*, *Math1*, *Nkx2.2*, *Mash1*, *Msx1*), embryonic liver (*Gata4*), TS cells (*Cdx2*), spleen (*Flk1*, *HoxA7*, *Gata1*), C2C12 cells (*Myf5*) and ES-OS25 (*Oct4*).

suggest that it mediates repression by functioning as a ubiquitin E3 ligase specific for histone H2A lysine 119 (refs 23, 24). To understand the role of Polycomb repressors in maintaining RNAP in a poised configuration, we used ES-ERT2, an ES cell line, that carries a tamoxifen-inducible, conditional knockout of the core PRC1 protein Ring1B, and is also homozygous null for the functional homologue Ring1A. Thus, following addition of tamoxifen, ES-ERT2 cells are progressively depleted of Ring1B protein and global H2A ubiquitination, whereas overall levels of PRC2 proteins and associated H3K27me3 are largely unaffected (Fig. 4a–d). Microarray expression analysis of ES-ERT2 cells following Ring1B deletion has demonstrated rapid de-repression of Polycomb target genes which, in turn, triggers widespread differentiation of ES-ERT2 cells approximately 3–4 days after addition of tamoxifen (M.V. and H.K., data not shown). Consistent with these findings, we observed de-repression of bivalent genes within 72 h of treatment (Fig. 4e). Notably, genes such as *Gata4*, *Nkx2.9* and *HoxA7* were markedly de-repressed within 48 h following addition of tamoxifen. In contrast, repression of the non-bivalent genes *Gata1* and *Myf5* was unaffected.

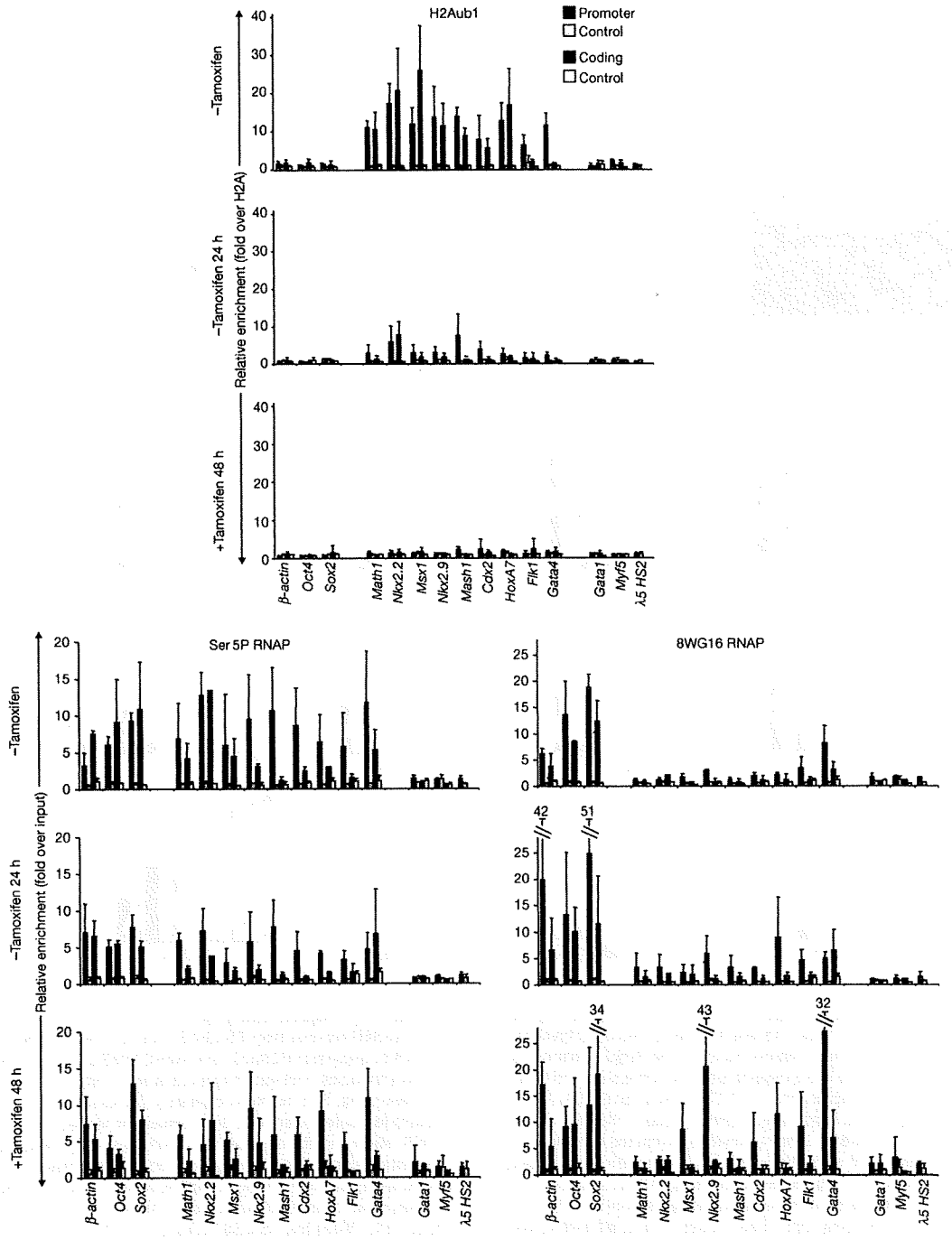

Figure 5 Loss of H2Aub1 results in changes in RNAP conformation at bivalent genes in ES cells. The abundance of H2Aub1, Ser 5P and 8WG16 RNAP was assessed at the promoter (blue bars) and coding regions (red bars) of bivalent genes after 0, 24 and 48 h tamoxifen treatment of ES-ERT2 cells to excise the *Ring1B* gene. Enrichment is expressed relative to input DNA using the same amount of DNA in the PCR and H2Aub1 is normalized to H2A. Background levels (mean enrichment from control antibodies and beads alone) at promoter and coding regions are shown as pale blue or white bars, respectively. Mean and standard deviations are presented from 3–4 independent ChIP experiments. Differences in abundance of H2Aub1, Ser 5P and 8WG16 RNAP at bivalent genes with time were statistically significant ($P < 0.0001$, $P = 0.02$ and $P = 0.002$, respectively; ANOVA).

Based on these observations, we examined early events occurring at bivalent gene promoters within the first 48 h following tamoxifen treatment and deletion of *Ring1B*. At this time ES-ERT2 cells remain undifferentiated, as validated by the continued expression of proteins such as Oct4, Nanog, Rex1, SSEA-1 and alkaline phosphatase (see Supplementary Information, Fig. S5). ChIP analysis demonstrated